The potential of QuikSCAT and WindSat observations for the estimation of sea surface wind vector under severe weather conditions

Y. Quilfen

Laboratoire d'Océanographie Spatiale, IFREMER, Plouzané, France

C. Prigent

Laboratoire d'Etude du Rayonnement et de la Matière en Astrophysique, Observatoire de Paris, Paris, France.

B. Chapron

Laboratoire d'Océanographie Spatiale, IFREMER, Plouzané, France

A. A. Mouche

Laboratoire d'Océanographie Spatiale, IFREMER, Plouzané, France

N. Houti

Laboratoire d'Etude du Rayonnement et de la Matière en Astrophysique, Observatoire de Paris, Paris, France

Corresponding author: Y. Quilfen, Laboratoire d'Océanographie Spatiale, IFREMER, BP70, 29280 Plouzané, France, yquilfen@ifremer.fr

Abstract. The physics of remote sensing sea surface measurements is still poorly understood under severe weather conditions. Wind vector algorithms are usually developed for non-precipitating atmospheres and for wind speeds less than 20 m/s. In this study, we analyze observations from the QuikSCAT Ku-band scatterometer collocated with the WindSat full polarimetric microwave radiometer to estimate the potential of these two instruments for sea surface wind retrieval under severe weather conditions. The Jason altimeter provides independent measurements of wind speed and rain rate for comparison purposes. The sensitivity of the radar cross-sections and brightness temperatures to the wind speed and direction is directly studied from the observations and compared with semi empirical models. This study clearly demonstrates that wind vector retrieval under extreme condition is feasible. Comparisons between QuikSCAT and WindSat coincident observations evidence a better sensitivity of the active mode to low and moderate winds and more sensitivity to high wind speeds in the passive mode. Although the WindSat observations are affected by water vapor, cloud, and rain, especially at and above 18 GHz, the measurements are sensitive to wind speed even at high wind speeds. Contrarily to the active instrument, there is no saturation at high winds. The sensitivity clearly tends to increase for winds above 15 m/s. For the wind direction, the amplitude of the azimuthal modulation in the active mode decreases with increasing wind speed, while it increases for the passive measurements. The development of specific wind retrievals under severe weather conditions is encouraged and a simple illustration is provided.

1. Introduction

No existing sensor has been specifically designed to probe the sea surface during extreme weather events and there is a need to elaborate from existing sensors. Already decided operational Earth observation missions for the coming 15 years include scatterometers (the Meteorological Operational, MetOp, satellite series) and microwave radiometers (the National Polar-Orbiting Operational Environmental Satellite System, NPOESS, and MetOp satellite series). A critical review of the scatterometer and microwave radiometer potentialities / limitations to measure the surface winds under severe weather conditions is thus necessary. The sensitivity of the various instruments to the extreme events has to be objectively analyzed, under the same conditions, i.e., when coincident observations of both instruments are available. This can further lead to potential synergies between active and passive measurements on future Earth observation missions. The recent satellite polarimetric measurements from WindSat (Gaiser et al., 2004), launched in January 2003 have not been completely explored yet and provide new information under high wind speed and / or intense rain.

The physics of remote sensing measurements over sea surface is still poorly understood under extreme conditions. Remote sensing at high wind speed is mostly controlled by the observation ability to directly or indirectly probe the wave breaking impacts. The wind vector algorithms are usually developed for non-precipitating atmospheres and for wind speeds less than 20 m/s. Preliminary evaluations of the first versions of the ocean wind algorithms from WindSat under hurricane conditions (Adams et al., 2006) concluded that the wind speed was strongly affected by heavy clouds and precipitation. However, these results were only obtained after less than 3 years of

WindSat operation and full use of the polarimetric information combined to innovative approaches should improve the retrievals (Adams et al., 2006). Concerning active measurements, the larger wave breaking signatures as well as foam and bubble impacts on the ocean surface dielectric and geometrical properties have been analyzed with altimeter measurements (Quilfen et al., 2006). At larger incidence angles provided by scatterometer observations, larger wave breakings can provide a very active source to generate shorter scale roughness (Kudryavtsev and Johannessen, 2004) to help maintain the wind speed sensitivity. Larger wave breaking events correspond to larger zones covered with foam. More interestingly, larger breakers are associated with thicker foam patches (Reul and Chapron, 2003). These two aspects (coverage and thickness) have significant impacts on passive radiometric measurements.

In this study, we analyze multi-sensor observations from the QuikSCAT Ku-band scatterometer collocated with the WindSat full polarimetric microwave radiometer. The Jason altimeter mission provides independent measurements of wind speed, rain rate, and atmospheric water content to help interpret the results. A systematic data screening tool has been developed to collocate the three different sensors within a given space / time window. The data are presented in section 2, with special focus on the rain flagging procedure. In section 3, the sensitivity of the radar cross-section and brightness temperatures to the wind speed and direction is studied from the observations and compared with semi-empirical model simulations, with emphasis on the high wind speed regime and on the effect of the atmospheric conditions. In section 4, the nominal wind vector retrievals from both WindSat and QuikSCAT are compared and presented to highlight the possible residual errors in the WindSat wind vector retrieval. Finally, in

section 5, retrievals using various observation combinations are tested, using both the radiometer and the scatterometer, to help analyze the information content of passive and active observations, and to show that the WindSat nominal wind speed retrieval can be improved to provide valuable estimates as well as to complement the radar measurements under severe weather conditions.

2. Data

2.1. The instrument characteristics

2.1.1. WindSat

Coriolis is a 3-year demonstration / validation mission sponsored by the Department of Defense Space Test Program, the U.S. Navy, and the National Polar-Orbiting Operational Environmental Satellite System (NPOESS) Integrated Program Office. It was launched on January 6, 2003, on a geosynchronous polar orbit, with ascending node at 17:59 UTC. WindSat onboard the Coriolis mission is a polarimetric microwave radiometer developed and built by the Naval Research Laboratory (NRL). Its objective is to demonstrate the potential of polarimetric measurements to estimate the ocean surface wind vector (speed and direction).

The measurement principle makes use of the natural microwave emission of the sea surface that varies with sea surface roughness. The rougher the sea, the more intense is the emission. The received energy is a combination of energy emitted from the ocean surface, from the atmosphere, and from the atmosphere reflected off the surface. WindSat is the first space borne polarimetric microwave radiometer. It measures not only the orthogonal polarizations (vertical and horizontal), but also the cross-correlation of the

vertical and horizontal polarizations. The cross-correlation terms represent the third and fourth parameters of the modified Stokes vector (U and F). The Stokes vector provides a full characterization of the electromagnetic signature of the ocean surface, and the independent information needed to determine the wind direction.

WindSat uses a 1.8-m offset reflector antenna fed by eleven dual-polarized feed horns. It operates at 6.8, 10.7, 18.7, 23.8, and 37 GHz, with 10.7, 18.7, and 37 GHz fully polarimetric (the four Stokes parameters are measured, V, H, U, and F) whereas the other channels are only measured in the two orthogonal polarizations (V and H). The Earth incidence angle is close to 53° (respectively 53.5°, 49.9°, 55.3°, 53.0° and 53.0° for each frequency) and the spatial resolution ranges from 40 km x 60 km at 6.8 GHz to 8 km x 13 km at 37.0 GHz. The expected accuracy is 0.75 K for the V and H channels and 0.25 K for the third and fourth Stokes parameters. A complete description of the instrument and its characteristics is given in Gaiser et al. (2004).

2.1.2. QuikSCAT

The SeaWinds instrument on QuikSCAT is an active microwave radar designed to measure the electromagnetic backscatter from the wind roughened ocean surface. The SeaWinds instrument uses a rotating dish antenna with two spot beams that conically sweep, producing a circular pattern on the surface. The antenna radiates microwave pulses at a frequency of 13.4 GHz. The antenna spins at a rate of 18 rpm, scanning two pencil-beam footprint paths at incidence angles of 46^{o} (H-pol) and 54^{o} (V-pol). The instrument collects data over ocean, land, and ice in a continuous, 1,800 km wide band centred on the spacecraft nadir ground track, covering 90% of Earth's surface each day.

Spaceborne scatterometers transmit microwave pulses to the ocean surface and measure the backscattered power received at the instrument. Since atmospheric motions themselves do not substantially affect the radiation emitted and received by the radar, scatterometers use an indirect technique to measure wind velocity over the ocean. Wind over the ocean generates ripples and small waves, which roughen the sea surface. These waves modify the radar cross-section (σ_o) of the ocean surface and hence the magnitude of backscattered power. In order to extract wind velocity from these measurements, a relationship between σ_o and near-surface winds, known as the geophysical model function, has to be established.

2.2. The collocation methodology and criteria

The "Centre ERS d'Archivage et de Traitement" (CERSAT) located at the "Institut Français de Recherche pour l'Exploitation de la Mer" (IFREMER, France) is a mirror site for the QuikSCAT data and thus manages the archive of levels 2A and 2B products for the complete QuikSCAT mission. CERSAT also archives the data from all scatterometer missions and most of the altimeter missions. The WindSat product version used for collocation with QuikSCAT and Jason is the last one delivered in 2006, version 1.9. At the end of July 2006, the SeaWinds project began producing QuikSCAT data to replace version 2.4, using new processing software that features an improved rain flag, a better performance at high wind speeds, and a 12.5 km wind vector retrievals for level 2 data. This improved data set is used in the present study.

CERSAT produced the WindSat / QuikSCAT and the WindSat / Jason collocated data set for the complete available WindSat data set, covering February 2003 to November

2005 with gaps. Sensors are collocated by pairs, WindSat with QuikSCAT and WindSat with Jason. The data from two sensors are collocated when the time difference is less than one hour and when their ground distance is less than 25 km. All parameters from the L2A (products containing instrumental data among which the radar cross-sections), L2B (products containing geophysical data, i.e., wind vector), SDR (products containing instrumental data among which the brightness temperatures), EDR (products containing geophysical data, i.e., wind vector and atmospheric parameters), or GDR (products containing both low level and geophysical data, i.e., wind vector, radar cross-sections) products are included in the collocated product, depending on which sensors are concerned. For this study, we use two months (February-March 2003) of WindSat / QuikSCAT collocated data for the analysis of the lower level data (radar cross-section and brightness temperature) and four months (February-May 2003) for the analysis of the wind data. Fifteen months (February 2003 - April 2004) of WindSat / Jason collocated data are also examined for comparisons.

2.3. The rain flag issue

Rain effects on passive and active microwave measurements depend on the sensing frequency and on the sensor measurement geometry. It has been shown (Tournadre and Quilfen, 2003) that the Ku-band QuikSCAT data are affected even by moderate rain rate. Measurements of the ocean surface σ_0 become contaminated for several reasons. Some of the transmitted energy is scattered back towards the scatterometer by the rain and never reaches the ocean surface. Energy backscattered from rain can constitute a significant portion of the measured echo energy. Some of the transmitted energy is scattered and / or

absorbed by the rain and is never measured by the scatterometer. This has the effect of attenuating the echo energy from the ocean. Additionally, the rain roughens the ocean surface and changes its radar cross-section. The total effect results in overestimation of the lower winds and underestimation of the higher winds (Tournadre and Quilfen, 2003). Two rain flags are included in the QuikSCAT Level 2B data to indicate detection of rain contamination. The mp_rain_probability is derived using the Impact-based Multidimensional Histogram (IMUDH) rain-flagging technique developed by Huddelston and Stiles at NASA JPL (2000). Briefly, mp_rain_probability from IMUDH does not flag a specific rain rate but a likelihood that the wind speed is perturbed by more than 2 m/s or the direction by more than 15°. The nof_rain_index is derived using the Normalized Objective Function (NOF) rain-flagging technique developed by Mears (2000). It is based upon a simplified version of the standard model function to determine a maximum likelihood estimator and a wind speed for each wind vector cell. In the present study, we use the mp_rain_probability (hereafter RP) since it was shown more efficient (Freilich and Vanhoff, 2006). A threshold of 0.2 for the QuikSCAT RP rain flag is a good compromise to flag the rain-contaminated QuikSCAT data and to avoid QuikSCAT high wind over-flagging (Tournadre and Quilfen, 2005).

The WindSat rain flag provided in the EDR products is used in the study. It is based upon a threshold of the 0.2 mm value for the Cloud Liquid Water content (hereafter CLW). An illustration of the rain flagging problem is provided in Figure 1. Indeed, as discussed in Tournadre and Quilfen (2005) using the precipitation radar data from the Tropical Rainfall Measuring Mission (TRMM), the RP rain flag is not self sufficient under high wind conditions. Due to WindSat / QuikSCAT time and space collocation

errors and high time and space rain cell variability, the WindSat CLW test may fail also to flag the QuikSCAT rain-contaminated data. Figure 1 displays the QuikSCAT wind speed as a function of the RP and CLW parameters (left) and the number of points in each RP / CLW bin (right). The two RP and CLW thresholds used for rain flagging are indicated. High values of RP are associated with mean high winds as measured by QuikSCAT. For RP values larger than about 0.8 the CLW content is greater than 0.2 mm, meaning that these points are clearly associated with rain in stormy conditions and detected by the two flags. Data with RP values between 0.2 and 0.8 and CLW values lower than 0.2 may be associated either to RP over-flagging or to CLW under-flagging. Accounting for the high space / time variability of rain events, possible CLW under-flagging may be due to the space / time difference between the QuikSCAT and WindSat measurements. Figure 1 (right) shows that for about 6% of the points the QuikSCAT flag is not set when the WindSat one is. It is impossible to distinguish between WindSat over-flagging due to space / time collocation errors and QuikSCAT under-flagging. The higher CLW values associated with mean high QuikSCAT winds could be both. For this reason and because both instruments are affected by rain, the two flags are often used jointly in the study: it corresponds to discard 8.3% of the collocated data.

2.4. Statistics of the winds in the collocated database

Figure 2 illustrates the spatial distribution of the collocated WindSat / QuikSCAT and WindSat / Jason observations. The WindSat / QuikSCAT collocated database covers most of the ocean with a larger concentration of match-ups at tropical and sub-tropical latitudes than at high latitudes where higher wind speeds are expected. Inversely, the

WindSat / Jason database covers mainly the high latitudes in southern oceans. This is inherent to the sensor geometries and orbital configuration. As a consequence, the results obtained in this study should be carefully analyzed with respect to these non uniform geographical distributions.

Figure 3 (top) shows the distribution of the QuikSCAT and WindSat retrieved wind speed and direction for the collocated database, along with the National Centers for Environmental Prediction (NCEP) model results (these histograms include only the pixels for which the WindSat wind speeds are estimated, i.e., excluding the rainy pixels). As expected, the wind speed distribution peaks around 7 m/s, with limited match-ups above 15 m/s, regardless of the wind information sources. The wind direction with respect to the North has two peaks, a large one around 270° (easterly winds) and a weaker one around 90° (westerly winds). The bottom panels on Figure 3 zoom on the high wind tail of the distribution and show that westerlies dominate for high wind speeds. The population of high wind speed retrieved by QuikSCAT is lower than the one estimated from the other sources.

3. Sensitivity of the passive and active measurements to the surface wind and comparison with semi-empirical models

The sensitivities of the active and passive instruments to the wind vector are analyzed from the satellite observations and compared with semi-empirical models. In this section, only the non-rainy observations are considered, as flagged from both QuikSCAT and WindSat (pixels declared rainy by QuikSCAT or WindSat are not considered).

3.1. The active responses

Asymptotic models (small perturbation and small slope approximation at first order, Kirchoff approximation or two-scale model) used to predict the normalized radar cross-section of the sea surface generally fail to reproduce in details backscatter radar measurements. In particular, the predicted polarization ratio versus incidence angle and azimuth angle is not in agreement with experimental data. This denotes the inability of the standard models to fully take into account the roughness properties with respect to the sensor configuration (frequency, incidence, and polarization).

One of the models (Mouche et al., 2007a) used in this study considers the latest improvements obtained in the field of approximate scattering theories of random rough surfaces using the local and resonant curvature approximations (RCA). The RCA model is based on an extension of the Kirchoff approximation up to first order to relate explicitly the curvature properties of the sea surface to the polarization strength of the scattered electromagnetic field. As shown in Mouche et al. (2007a), dynamically taking into account the sea surface curvature properties is crucial to better interpret normalized radar cross-section and polarization ratio sensitivities to both sensor characteristics and geophysical environment conditions. The validation of the RCA model, presented in Mouche et al. (2007b), makes use of NSCAT Ku-band scatterometer data and aircraft C- and X-band data acquired during stormy conditions. It shows significant improvement obtained in modelling the polarization ratio with the RCA model as compared with the classical approaches.

The second model used to compare with QuikSCAT data assumes a decomposition for the sea surface. Following Quilfen et al. (1999), Kudryavtsev et al. (2003) decomposed the normalized radar cross section (σ_0) as a sum of two terms. The regular surface is associated with the Bragg scattering theory whereas zones of enhanced roughness associated to the presence of individual breakers contribute to the radar signal through non polarized, scalar, contributions. The Bragg scattering theory is taken into account by a two-scale model. Note that this model has also been developed to corroborate the NSCAT data.

Figure 4 presents the comparison between the QuikSCAT normalized radar cross-section σ_0 and those estimated using the RCA and Kudryavtsev models, as a function of wind speed. σ_0 increases quickly with the wind speed at low to moderate winds, then saturates with increasing wind speed. The RCA model indicates a full saturation, while the data still show some sensitivity with increasing wind speed. The Kudryavtsev model fits the data slightly better at high winds. Inclusion of enhanced roughness areas (linked to breakers) in the surface description certainly helps increase the σ_0 sensitivity to high winds. The modeled and measured polarization differences are in good agreement for both models, although larger than shown in the data beyond 25 m/s for the Kudryavtsev model. It decreases with increasing wind speed from moderate to about 20 m/s, because the HH polarization shows slightly better sensitivity with increasing winds. The Kudryavtsev model reproduces the crossing of the HH (46^o incidence angle) and VV (54^o incidence angle) curves near 20 m/s. Faster decreasing sensitivity of the σ_0 VV with increasing wind speed beyond 25 m/s was also found by Fernandez et al. (2006) using airborne scatterometer and radiometer data during tropical cyclone events. They

measured approximately a 4 dB (2 dB) σ_0 increase at HH (VV) for winds increasing from 25 to 60 m/s.

The dependence of the mean σ_0 on the wind direction is shown in Figure 5, for VV (top panel) and HH (bottom panel) polarizations, for the RCA model (blue curves) and the data (red curves), at 6, 14, and 22 m/s. Only the RCA model results are presented for the anisotropic part because the Kudryavtsev model in its present form does not account for a wind speed dependence of the azimuthal modulation. The data and the RCA model are in relative good agreement at HH polarization, but the amplitudes of the azimuthal modulation differ significantly at VV polarization. The RCA model indicates dramatic increase of the modulation with increasing wind speed while data feature slightly decreasing modulation. This is also true at HH polarization, but to a smaller extent. Such apparent discrepancies are mainly due to the statistical surface description used to compute the RCA predictions. Adjustments could certainly be made but are beyond the scope of this study. RCA predicts larger HH cross-section than any other asymptotic scattering model and fits the measurements better. Moreover, the RCA model tends towards a Kirchoff asymptotic relation at high winds, i.e. the sea surface polarization sensitivity strongly decreases. At the extreme, both VV and HH predictions match. Careful analysis shall be directed to data showing larger HH measurements than VV ones. Indeed, this necessarily indicates distinct scattering mechanisms to be possibly attributed to breaking event effects.

3.2. The passive responses

The passive microwave observations are sensitive to the sea surface as well as to the atmosphere. To quantify the brightness temperature (Tb) behaviour, we computed their mean values averaged into wind speed bins and for three different integrated water vapor (WV) ranges. This is illustrated in Figures 6 and 7. Only the three lower frequencies are described in these figures since they are less affected by the atmosphere. The behaviour of all 5 frequencies will be described later in this section. Figure 6 displays the mean values using the WindSat / Jason database, where the wind speed reference is the ECMWF one and the WV reference is either the WindSat one (solid lines) or the Jason Microwave Radiometer one (JMR, dashed lines) for comparison purpose. Figure 7 displays the same features with the QuikSCAT wind speed and the WindSat WV values as references. It can be seen that the results agree very well when using indifferently the Jason or WindSat WV data and the QuikSCAT or ECMWF wind speed. The most striking feature is that the H polarization is more sensitive to the wind that the V polarization. The V polarization also appears related to the water vapor content, especially at 6.8 and 18.7 GHz. This is expected from the 18.7 GHz but not from the 6.8 GHz channel: the 6.8 GHz is actually sensitive to the sea surface (SST) temperature that is usually correlated with the integrated water vapor in the atmosphere. From RTTOV model simulations with a wind speed of 7m/s and for a typical tropical atmosphere, the change in Tb due to a SST increase of 1 K is of the order of 0.6K (resp. 0.4K) at 6 GHz for the V polarization (resp. H). It is twice less at 18 GHz and keeps decreasing with frequency. Most of the high WV content data are associated with moderate winds and the winds larger than 10 m/s are generally associated with low WV values. The H-pol Tb's

increase quickly with the wind speed and do not present any saturation at wind speed greater than 20 m/s, whatever the WV range. There is roughly a 1K per 1 m/s slope, slightly larger for winds above 12 m/s as it can be seen mainly at 6.8 and 10.7 GHz. This change in the slope is much more pronounced in the V-pol data: the Tb's are not very sensitive to wind speed increase from low to moderate winds. Indeed, at 53° incidence angle (which is close to the Brewster angle for sea water in this frequency range), the V-pol signal is not very sensitive to the surface roughness. The change in V-pol is essentially due to the presence of foam that changed with wind speed. The foam coverage increase with wind speed is exponential in shape in most models (e. g., Monahan and O'Muircheartaigh, 1986), similar to the observed change in the V-pol signal with wind speed. The V-pol wind speed sensitivity seems reduced in presence of high integrated water vapor content. The 18.7 GHz channel is much more sensitive to the WV content than to the wind speed, especially for V-pol with a difference of roughly 25 K at 10 m/s between the two extreme WV ranges, while it is only 8 K at lower frequencies.

The WindSat / QuikSCAT database is our primary source for comparison between passive and active measurements under severe weather conditions because it contains more high wind speed observations. To further justify the use of QuikSCAT wind speed as reference, rather than NCEP also available in the database, Figure 8 presents the brightness temperature standard deviations (SD's) for wind speed bins, when QuikSCAT and NCEP wind speeds are used as reference. A water vapor threshold of 20 mm has been applied to minimize the atmospheric contribution to the Tb's variability. The SD's values contain information on the variability of the other geophysical parameters (SST, salinity, waves) into 2m/s bins but also contain information on the correlation between

the chosen reference wind speed and the brightness temperature. The lower the SD's, the better the correlation between wind speed and Tb, the better the wind speed reference. It can be seen that the SD's are generally lower when the satellite winds are used, for winds beyond 10 m/s. The SD's increase with increasing channel frequency. The lowest SD's obtained with the QuikSCAT winds justify the subsequent use of QuikSCAT for the evaluation of the WindSat radiometric measurements.

Figure 9 illustrates the Tb's behavior as a function of wind speed for the five WindSat channels. For comparison purposes, the sea surface emissivity model FASTEM-3 (English and Hewison, 1998; Deblonde, 2000) from the RTTOV fast radiative transfer model has been used (Eyre, 1991; Matricardi et al., 2004). The development of the RTTOV fast radiative transfer model is part of the EUMETSAT sponsored NWP-SAF activities. The last RTTOV-8 version includes the capability to simulate polarimetric radiometers (e.g., WindSat). In line with the semi-empirical model developed by Kudryavtsev and his co-authors (2003), FASTEM-3 uses a two-scale ocean roughness approximation and takes explicitly into account emissivity from foam patches. The ocean permittivity is derived from Ellison et al. (1998) and the foam coverage calculated from Monahan and O'Muircheartaigh (1986). The azimuthal dependence from Liu and Weng (2002, 2003) is adopted in FASTEM-3, but with revised coefficients derived from the model presented by Coppo et al. (1996) that predicts reduced amplitude of the azimuthal dependence. Tb's have been computed for a dry (4 mm of water vapor content and a SST of 10^{o} C) and a wet (40 mm of water vapor content and a SST of 26^{o} C) atmospheres. From the WindSat observations, dry (wet) cases have been selected using measurements for which the integrated water vapor content is in the 0 to 20 mm (20 to 60 mm) range,

and the distribution has been adjusted in order to obtain a mean SST of 10^{o} C and 26^{o} C for the dry and wet atmospheres, respectively. The general agreement between WindSat and RTTOV is good, although the mean Tb difference for the two water vapor ranges is generally greater for RTTOV, as expected by the fact that the selected atmospheres for the simulations corresponds to extreme cases, especially for the dry atmosphere. However, the sensitivity to the wind speed is well reproduced although there is a faster increase in H-pol at high wind speeds for the model simulation. This difference is channel dependent and is larger at lower frequencies. As previously noted, the model confirms that there is no saturation of the brightness temperatures at high wind speeds. There are few data beyond 25 m/s, but the RTTOV model indicates continuous increase in Tb's beyond 30 m/s. This is exclusively due to the foam coverage parameterization, i.e, Monahan and O'Muircheartaigh (1986), and may certainly be questioned, e.g., the foam coverage percentage exceeds 100% beyond 40 m/s. It may explain the faster increase of the H-pol RTTOV simulations by comparison with data.

The 3^{rd} (U) and 4^{th} (F) Stokes parameters are computed for the 10.7, 18.7, and 37.0 GHz channels. Sensitivity of these parameters to the wind direction has been quantified (Yueh et al., 2006). Figures 10 and 11 further illustrate this sensitivity in case of a dry (Figure 10) and a wet (Figure 11) atmospheres as selected from the data to outline that these parameters are little affected by the atmosphere contrarily to the two first Stokes parameters. The azimuthal modulation increases with wind speed up to 18 m/s and does not vary significantly for winds beyond 20 m/s (red curves). Still, the scarcity of high wind data does not enable confident estimates of the modulation intensity. A small phase shift is apparent in the signal as the wind speed increases, already noted in Yueh et al.

(2006). The maximum amplitude of 4 K (U) and about 0.7 K (F) at 18.7 GHz for wind speed higher than 16 m/s is consistent with the Yueh et al. results. As expected, the 1st harmonic dominates in the U modulation, with decreasing 2nd harmonic modulation with increasing frequency, while the 2nd harmonic is predominant in the F modulation. The F signal is less than 0.2 K at 37.0 GHz and is almost unusable. U thus exhibits a strong upwind / downwind modulation while F exhibits a strong upwind / crosswind modulation.

The azimuthal modulation remains almost unchanged in case of a wet atmosphere (Figure 11) although its amplitude slightly decreases. Sensitivity of the U and F Stokes parameters to the wind direction is not affected by atmospheric contribution, even at 37 GHz. From aircraft observations with the WINDRAD instrument (17, 19, and 37 GHz), Yueh et al. (2006) also observed that the radiometric wind direction information was robust to weather conditions, with similar response from 17 to 37 GHz, even at wind speed above 20 m/s.

Figure 12 presents a comparison between WindSat and the azimuthal modulation from the RTTOV model. The model reproduces quite well the azimuthal modulation but shows also systematic differences with the WindSat data. It features much larger amplitudes for F. It predicts an increase of the modulation from low to high winds in agreement with data for U but this increase is not present in the data for F. For F, the RTTOV model modulation is almost the same regardless of the channel whereas the data show much weaker modulation at 37 GHz. For U, the RTTOV model modulation is decreasing with increasing frequency whereas the data show nearly constant azimuthal modulation amplitude. The distribution of the first and second harmonics is comparable for F for

which the upwind / crosswind modulation dominates for both model and data. It differs for U for which the data show increasing (decreasing) upwind / downwind (upwind / crosswind) modulation with increasing frequency whereas RTTOV has the opposite behavior. Finally, but not surprisingly, the disagreement is larger for higher winds for which there are significant differences in the amplitude and phase of model and data azimuthal modulations.

3.3 Discussion

It is worth reminding that physical models are generally developed to account for mechanisms taking place under average weather conditions. It is thus not surprising that extrapolation to severe weather conditions does not compare very well with data. However, the good agreements obtained in the mean behavior of the simulations, for both active and passive modes, are stimulating to pursue efforts in the physical modeling field. Note that the RCA model is developed in a way that enables its extension to passive measurements. Such a synthetic tool will help better analyze the active / passive measurements, with a consistent approach under extreme weather conditions.

Under high wind conditions, the sea surface is no longer simply related to the wind speed. In winds approaching hurricane strength, an enhanced breaking activity is taking place at the surface of the ocean. Both whitecaps and spray droplets proliferate, as well as intense mixing of the surface waters with turbulent transport of bubbles to depth. Whitecap bubbles and sea spray provide additional surfaces and volumes that may impact the transfer of any quantity normally exchanged at the air–sea interface. The key parameterization to describe the ocean surface dynamics under such extreme conditions is the distribution of the total length of breaking fronts moving with a given speed or having

a certain wavelength scale. As it can be expected, under extreme wind forcing, breaking waves are distributed over a wider range of surface wave scales as compared to more gentle conditions. As larger waves are involved in breaking processes, both foam coverage and foam thickness significantly increase with increasing wind speeds (Reul and Chapron, 2003). This is certainly the main principle leading to passive measurement sensitivities to high wind conditions. Further, spume drops torn off breaking crests are sprayed inside the air flow at higher height, i.e., the larger scale mean height, to possibly significantly affect the turbulent mixing. This latter effect can then lead to acceleration of the air flow and reduction of the surface drag, as suggested by recent wind profiles measurements under hurricane wind conditions (Powell et al., 2003). Consequently, ocean surface passive remote sensing measurements at very high wind speeds are certainly well adapted and mostly controlled by the instrument abilities to directly or indirectly probe the larger wave breaking impacts. Emissivity models as well as measurements predict saturation in foam emissivity, i.e., foam approaches the behaviour of a black body, for sea-foam thickness larger than about 2 times the electromagnetic wavelength (Rose et al., 2002; Reul and Chapron, 2003). Passive measurements below 15 GHz, and to lesser extent at higher frequencies, are thus expected to provide interesting measurements under very high wind speeds (> 30 m/s). This is confirmed by the WindSat measurements. Concerning active measurements, these larger wave breaking signatures as well as foam and bubble impact on the ocean surface dielectric properties have apparently been successfully captured with altimeter measurements (Quilfen et al., 2006). At low incidence angle, large wave geometry can indeed contribute to the signal sensitivity. At backscatter geometry with larger incidence angle, larger wave breakings

have indirect effects to provide a very active source to generate shorter scale roughness (Kudryavtsev and Johannessen, 2004), and thus to maintain the sensitivity of the radar cross-section to wind speed as shown in Figure 3 for the Kudryavstev semi-empirical scattering model. This source may thus somehow compensate the plausible reduction of small scales direct wind generation, associated to the predicted surface drag reduction. Furthermore, sharply crested waves can also directly enhance the mean backscatter measurements, e.g., increasing radar sea spikes. Following these considerations, backscatter measurements will not be fully saturated at very high wind speeds, as confirmed from QuikSCAT or aircraft radar measurements (Fernandez et al., 2006). However, in such a configuration, measurements shall be made at higher incidence, possibly in horizontal polarization. The electromagnetic wavelength choice is not expected to be crucial under extreme conditions to efficiently probe the ocean surface. To avoid precipitation effects, measurements at lower frequencies (C- and L-bands) should be considered. Finally, as the ocean surface is expected to exhibit localized and intermittent processes, both passive and active estimates should not solely rely on the mean instrumental measurement levels. To better characterize the expected randomness of the fluctuating measurements under hurricane conditions, attention could also focus on the higher order statistics, in particular the variance of the measured signals. Fluctuations of both brightness temperatures and radar cross-sections inside stormy area have generally been reported to vary a lot, with the normalized variance of the signals increasing with wind speeds.

Comparisons between QuikSCAT and WindSat sensitivity to the wind speed evidence a better sensitivity of the active mode to low and medium winds and more sensitivity to

high wind speed in the passive mode. QuikSCAT sensitivity to winds beyond 20 m/s, as verified from few field experiments (Fernandez et al., 2006), is low and estimation of extreme events intensity is thus difficult. On the other hand, this study illustrates the very good sensitivity of WindSat to high winds, as also observed from the nadir viewing Stepped Frequency Microwave Radiometer, SFMR (Fernandez et al., 2006). However, WindSat being sensitive to surface temperature at low frequencies and to water vapor, clouds and rain at higher frequencies, these variables have to be estimated separately. Measurements from channel combinations have certainly to be used to extract the wind information from these passive microwave observations.

4. Analysis of the retrieved WindSat and QuikSCAT wind vector

In this section, the WindSat and QuikSCAT wind retrievals from the operational algorithms are compared, with special focus on the estimates under extreme weather conditions.

4.1. Wind speed comparison

Figure 13 presents the distribution of the WindSat minus QuikSCAT wind speed differences for non-rainy pixels. The mean WindSat minus QuikSCAT difference is 0.26 m/s and the standard deviation 0.89 m/s, with maximum and minimum values of 32 m/s and -16 m/s, respectively. Figure 13 middle and bottom panels show the WindSat and QuikSCAT wind speed distribution, respectively, for data for which the absolute value of the wind speed difference is greater than 8 m/s. While the distribution of the QuikSCAT wind speed is close the global mean wind speed distribution, the corresponding WindSat distribution is shifted towards high wind speed values. It corresponds mostly to WindSat

wind speed overestimation due to atmospheric effects as already outlined in Freilich and Vanhoff (2006). These data are filtered out for subsequent analysis. The new mean difference and standard deviations are 0.25 m/s and 0.79 m/s, respectively.

Mean WindSat speeds binned by QuikSCAT wind speeds are presented in Figure 14, for different WV content intervals. Data are filtered out for rain and for absolute wind speed difference larger than 8 m/s. The results are quite similar with those obtained in Freilich and Vanhoff (2006), although they did not analyze the effect of water vapor content and used an older version of the WindSat products (NESDIS0). They also found WindSat underestimation of high winds by a larger amount. Figure 14 shows that WindSat winds are lower than QuikSCAT in clear sky and high wind conditions and higher than QuikSCAT winds beyond 15 m/s in presence of high water vapor content. The dependence of the comparison on WV may be interpreted as a residual error of the WindSat winds due to multi-parameter retrieval algorithm errors in high winds and water vapor content conditions. For the wind speed range below 15 m/s, good agreement is found between QuikSCAT and WindSat.

Another validation is performed and illustrated in Figure 15 using the Jason and ECMWF winds available using the WindSat / Jason collocated data set. Results are slightly different from those obtained with the QuikSCAT comparison. We find a good agreement between WindSat and Jason or ECMWF wind speed whatever the wind speed range in clear sky conditions, although WindSat winds are slightly higher than the two other wind sources. The dependency of the observed wind speed difference on increasing water vapor is still apparent although less clear because there are few measurements beyond 15 m/s wind speed and 20 mm integrated water vapor. Indeed the collocated

WindSat / Jason measurements are found mainly in mid-latitudes while the collocated WindSat / QuikSCAT measurements are essentially found in tropical areas (Figure 2).

To conclude, good agreement is found between the WindSat and the QuikSCAT / Jason / ECMWF winds, except for winds greater than about 17 m/s for which WindSat winds are apparently lower than QuikSCAT winds. A residual dependency of the WindSat winds on the water vapor appears for winds beyond 15 m/s.

4.2. Wind direction comparison

Figure 16, from top to bottom, presents the standard deviation of the difference between the WindSat wind direction and the QuikSCAT, NCEP, and ECMWF wind direction, respectively. Standard deviations (hereafter SD) have been computed for different WV ranges and separately for the tropical and mid-latitude areas in order to account for the mean SST variability. Data for which the direction difference is greater than ninety degrees are discarded before estimation of the SD values. The comparison with the three different data sources shows that the wind direction SD is greater for mid-latitudes. It can be mainly explained as the result of the larger space / time variability in mid-latitude areas, thus associated with larger collocation errors. The SD is larger than 20° at low wind speeds and decreases quickly with increasing wind speed to reach values lower than 10°. SDs computed with QuikSCAT winds decrease faster which denotes the higher QuikSCAT wind direction accuracy for medium winds. The comparison with ECMWF provides still decreasing SD's for increasing wind speed beyond 15 m/s while comparison with QuikSCAT and NCEP shows slightly increasing SD values. It must be noted that there are few ECMWF wind speed data beyond 20 m/s. The comparison between the three data sources show that the SDs are lower than 10° for winds from 10

m/s to 20 m/s. This is an excellent agreement, better than the previous WindSat accuracy estimates that were of the order of 15^{o} in this wind speed range using the former version (NESDIS0) of the WindSat products (Monaldo, 2006; Freilich and Vanhoff, 2006). WindSat version 1.9 product are thus a significantly improved over the former ones.

The comparison between QuikSCAT and NCEP shows the effect of WV on the wind direction retrieval accuracy, as for the wind speed analysis. This effect is not clear in the comparison with ECMWF. This is attributed to the different WindSat / QuikSCAT and WindSat / Jason sampling (Figure 2). Although WindSat polarimetric measurements are not much affected statistically by the atmosphere, as shown in Figure 11, the higher scatter observed for higher water vapor content is certainly associated with the low signal to noise ratio for polarimetric measurements. Indeed the azimuthal signal is of the order of a few Kelvin. It is also not surprising that the mean SST conditions influence the magnitude of the scatter to induce differences in the comparison between WindSat and QuikSCAT, and WindSat and Jason measurements. Moreover, any error in the estimation of one of the other parameters (wind speed, WV, SST) will affect the wind direction retrieval of the multi-parameter retrieval process.

Figure 17 illustrates the difficulty of WindSat wind vector retrieval under stormy conditions. The top left (right) panel gives the rain free QuikSCAT (WindSat) wind field using the standard rain flag for each product. The bottom left (right) panel gives the WindSat integrated water vapor content (rain rate). The 0.2 mm threshold on the cloud liquid water content eliminates large interesting parts of the storm in the WindSat estimates. Despite this severe screening, there are still pixels with anomalous wind speed

values on the south side of the storm. WV is equal or greater than 50 mm over the displayed area. Wind vector retrieval under stormy conditions thus remains a challenge.

5. Statistical analysis of the information content of the satellite observations for surface wind retrieval under extreme conditions

Different algorithms have been developed to retrieve the wind speed and direction from the WindSat observations, ranging from physical models based on simulations to purely statistical schemes relying on collocations with buoys. All the channels are not systematically used. For instance, Bettenhausen et al. (2006) used a two step variational estimation coupled to an efficient forward physical model to estimate first the wind speed, the water vapor and liquid columns, and the surface temperature, and then the wind direction. T_H at 6.8 GHz and T_F at 37 GHz are excluded. On the other hand, Brown et al. (2006) developed an empirical wind vector retrieval scheme based on collocation between QuikSCAT and WindSat.

In order to assess the potential of the passive and active microwave observations for wind speed retrieval at high wind speeds, we attempt to reproduce the QuikSCAT wind speed (assumed to be the reference wind speed) with different observation combinations. A multi-linear regression algorithm is adopted. In a preliminary attempt, the training data set used the natural wind speed distribution in the initial database (Figure 3). This resulted in large biases in the retrieval of the high wind speed, due to the heavy weight of wind speeds around 7m/s in this database. It was thus decided to weight the contribution of the different wind speed to obtain the same proportion of all wind speed categories in the database. The following results are obtained with this 'uniformed' database. For each

observation combination, the statistics of the difference with the expected winds are calculated. They are a measure of the potential of this specific combination to retrieve wind speed. These statistics are examined under high wind speed and rainy situations, in order to assess the robustness of the retrieval under these conditions.

Figure 18 shows the results of the retrieved Windsat wind speed as compared to the operational QuikSCAT wind speed (QuikSCAT wind speed minus the new estimated wind speed) using 1) all the WindSat channels, 2) the WindSat channels without the 6.8 GHz, 3) WindSat without the 6.8 and 10.7 GHz channels, 4) all WindSat and QuikSCAT observations together, 5) for comparison purposes, the wind speed provided in the standard Windsat products. Table 1 gives the statistics of the estimates separating the rainy and non-rainy cases, and the high wind speeds. Note that the statistics presented in Figure 18 and in Table 1 are calculated on the original database, not on the 'uniformed' database. As expected from the 'uniformed' database used for the training of the algorithm, the performance of the retrieval is rather equivalent for all wind speed ranges. The WindSat observations reproduce well the QuikSCAT wind speed up to 25 m/s. Above 20 m/s, part of the discrepancy comes from the lack of high wind speed in the database: although the database has been 'uniformed' for the training of the statistical algorithm, at high wind speeds, the same samples are used many times, thus the variability of the sample is not natural and might be unrealistic. However, it shows that contrarily to the original algorithm that are tuned to be optimum for the most probable winds (around 7 m/s), this simple algorithm performs well in the upper wind speed range, above 15 m/s. Given that the observations are sensitive to the wind speed without saturation to high wind, optimized algorithms designed for high wind speed conditions

can be developed and this little experiment proves it. Nevertheless, note that a residual bias is observed for the most common winds around 7 m/s with the simple algorithm developed here (overestimation of the retrieved wind as compared to the QuikSCAT reference): it would be possible to develop different wind speed algorithms, depending upon the wind speed ranges, based on a prior classification of the situations. From Figure 18, it appears that the 6 GHz channels do not provide significant additional information (with or without these channels, the retrievals are very similar), but the 10 GHz channels have a significant impact. Adding QuikSCAT to the WindSat observations does not significantly change the results (note that if in Table 1 the rms is worse with QuikSCAT than without it is related to the fact that the algorithm is not trained on the database that is used to calculate the statistics, otherwise, adding information would make the statistic similar or better).

6. Conclusion and perspectives

Under extreme weather conditions, accurate wind vector retrieval is difficult for four main reasons. First, under high wind conditions, the sea surface is no longer simply related to the wind speed. Breaking activity and associated whitecaps and spray taking place at the surface of the ocean and interfere with the satellite response. There are ongoing efforts to understand and model these complex effects. Second, both physical models and wind vector retrieval methods have been primarily developed for medium range wind conditions, that are much more common. Third, extreme weather conditions are generally associated with clouds and rain that contaminate the satellite signal. The impact of these perturbations increasing with increasing observation frequency. Freilich and Vanhoff (2006) set the tone: ‘Accurate wind retrievals are not possible at all in heavy

rain'. Not only the rain in the atmosphere absorbs and scatters the microwave response but the rain drops on the ocean surface also affect the ocean roughness. Fourth, in high wind conditions, the wind speed can vary greatly over the satellite footprint. Therefore, the retrieval is really an average over the footprint and one often miss to measure the extreme winds because of this smoothing effect.

However, this study shows that wind vector retrieval under extreme condition is feasible. Comparisons between QuikSCAT and WindSat observations show that the active mode is more sensitive to low and moderate winds whereas the passive mode responds better to high wind speeds. Although the WindSat observations are affected by water vapor, cloud, and rain, especially at and above 18 GHz, the measurements are sensitive to wind speed even at high wind speed. Contrarily to the active instrument, there is no saturation at high winds and the sensitivity clearly increases for winds above 20 m/s. Developments of wind retrieval from WindSat observations could thus certainly be adapted to high wind speeds. As a first attempt, a multi-linear regression retrieval is presented in this study to show consistent and encouraging results, even under extreme conditions (high rain rate). For the wind direction, the amplitude of the azimuthal modulation in the active mode decreases with increasing wind speed, while it increases for the passive measurements. This also favours the use of WindSat for the estimation of the direction of high winds. However, given the limited amplitude of the signals, a good instrument accuracy has to be achieved (of the order of 0.2 K) to retrieve accurate wind direction from the polarimetric measurements (English et al., 2006). We only briefly tested the joint use of passive and active mode for wind speed retrieval. This possibility

should be examined further, to benefit from the different sensitivity of the two modes to the various wind speed ranges.

The main problem for the development of retrieval methods adapted to high wind speed lies in the lack of wind references under extreme conditions. This implies the need to develop dedicated collocated database. This also encourages the use of sea state information to trace efficiently the resulting scattered large swell conditions from localized extreme conditions, to better analyze extreme events intensity.

Acknowledgments:

This study has been partly funded by the European Space Agency in the frame of the Extreme Weather Events project. The Windsat data has been provided by the Naval Research Laboratory in the frame of the Windsat calibration/validation activities. The CERSAT, IFREMER, has produced the Windsat/QuikScat/Jason collocated products. The authors would like to thank Pascal Brunel and Stephen English for their help with the RTTOV model, Fuzhong Weng for providing the Liu and Weng emissivity model, and Jean Tournadre for helpul discussion.

References

Adams, I. S., C. C. Henneon, W. L. Jones, and K. A. Ahamad (2006), Evaluation of hurricane ocean vector winds from WindSat, *IEEE Trans. Geo. Sc. Remote Sens., 44,* 656-667.

Bettenhausen, M. H., G. K. Smith, R. M. Bevilacqua, N.-Y. Wang, P. W. Gaiser, and S. Cox (2006), A nonlinear optimization algorithm for WindSat wind vector retrievals, *IEEE Trans. Geo. Sc. Remote Sens., 44*, 597-610.

Brown, S. T., C. S. Ruf, and D. R. Lyzenga (2006), An emisisvity-based wind vector retrieval algorithm for the WindSat polarimetric radiometer", *IEEE Trans. Geo. Sc. Remote Sens., 44*, 611-621.

Coppo, P., J.T. Johnson, L. Guerriero, J.A. Kong, G. Macelloni, F. Marzano, P. Pampaloni, N. Pierdica, D. Solimini, C. Susini, G. Tofani, and Y. Zhang (1996), Polarimetry for passive remote sensing, ESA contract 1146/95/NL/NB, Final report.

Deblonde, G. (2000), Evaluation of FASTEM and FASTEM-2, *NWP SAF Report*, http://www.metoffice.com/research/interproj/nwpsaf/rtm/.

Ellison, W., A. Balana, G. Delbos, K. Lamkaouchi, L. Eymard, C. Guillou, and C. Prigent (1998), New permittivity measurements and interpolation functions for natural sea water, *Radio Sc.*, *33*, 668-685.

English, S. J., and T.J. Hewison (1998), A fast generic millimetre wave emissivity model, *Microwave Remote Sensing of the Atmosphere and Environment Proc. SPIE* 3503, 22-30.

English, S., B. Candy, A. Jupp, D. Beddington, S. Smith, and A. Holt (2006), An evaluation of the potential of polarimetric radiometry for numerical weather prediction using QuikSCAT, *IEEE Trans. Geo. Sc. Remote Sens*., *44*, 668-675.

Eyre, J. R. (1991), A fast radiative transfer model for satellite sounding systems, *ECMWF Research Dept. Tech. Memo.176* (available from the librarian at ECMWF).

Fernandez, D. E., J. R. Carswell, S. Frasier, P. S. Chang, P. G. Black, and F. D. Marks (2006), Dual-polarized C- and Ku-band ocean backscatter response to hurricane-force winds, *J. Geophys. Res*., *111*, C08013, doi:10.1029/2005JC003048.

Freilich, M. H., and B. A. Vanhoff (2006), The accuracy of preliminary WindSat vector wind measurements: Comparisons with NDBC buoys and QuikSCAT, *IEEE Trans. Geo. Sc. Remote Sens.*, *44*, 622-637.

Gaiser, P. W., K.M. St Germain, E.M. Twarog, G.A. Poe, W. Purdy, D. Richardson, W. Grossman, W.L. Jones, D. Spencer, G. Golba, J. Cleveland, L. Choy, R.M.

Bevilacqua, P.S. Chang (2004), The WindSat spaceborne polarimetric microwave radiometer: Sensor description and early orbit performance, *IEEE Trans. Geo. Sc. Remote Sens.*, *42*, 2347-2361.

Huddelston, J. N., and B. W. Stiles (2000), Multidimensional histogram (MUDH) rain flag, *Jet Propulsion Laboratory, California Institute of Technology*.

Kudryavtsev, V., and J. Johannessen (2004), Effect of wavebreaking on spectrum of short wind waves, *Geophys. Res. Let*., *31*, L20310.

Kudryavtsev V., D. Hauser, G. Caudal, and B. Chapron (2003), Semi-empirical model of the normalized radar cross-section of the sea surface. 1. Background model, *J. Geophys. Res*., *108*, 8054, doi: 10.1029/2001JC001003.

Liu, Q., and F. Weng (2002), A microwave polarimetric two-stream radiative transfer model, *J. Atmos. Sci*., *59*, 2396-2402.

Liu, Q., and F. Weng (2003), Retrieval of sea surface wind vectors from simulated satellite microwave polarimetric measurements, *Radio Sc*., *38*, 8078, doi:10.1029/2002RS002729.

Matricardi, M., F. Chevallier, G. Kelly, and J.N. Thépaut (2004), An improved general fast radiative transfer model for the assimilation of radiance observations, *Quat. J. Roy. Meteor. Soc., 130,* 153-173.

Mears C. (2000), Sea Winds on QuikSCAT normalized objective function rain flag, version 1.2, 13pp, Remote Sensing System, Santa Rosa, Calif.

Monahan, E. C., and I. O Muircheartaigh (1986), Whitecaps and the passive remote sensing of the ocean surface, *Int. J. Remote Sensing*, *7*, 627-642.

Monaldo, F. M. (2006), Evaluation of WindSat wind vector performance with respect to QuikSCAT estimates, *IEEE Trans. Geo. Sc. Remote Sens*., *44*, 638-644.

Mouche, A., B. Chapron, and N. Reul (2007a), Asymptotic theory for ocean surface electromagnetic waves scattering, in press in *Waves in Random and Complex Media*.

Mouche, A., B. Chapron, N. Reul, D. Hauser, and Y. Quilfen (2007b), Importance of the sea surface curvature to interpret the normalized radar cross-section, submitted to *J. Geophys. Res*.

Powell, M. D., P. J. Vickery, and T. A. Reinhold (2003), Reduced drag coefficient for high wind speeds in tropical cyclones, *Nature*, *422*, 279-283.

Quilfen, Y., B. Chapron, T. Elfouhaily, K. B. Katsaros, and J. Tournadre (1998), Observations of tropical cyclones by high-resolution scatterometry, *J. Geophys. Res.*, *103*, 7767–7786.

Quilfen, Y., B. Chapron, A. Bentamy, J. Gourrion, T. Elfouhaily, and D. Vandemark (1999), Global ERS-1/2 and NSCAT observations: upwind/downwind and upwind/crosswind measurements. *J. Geophys. Res.*, *104*, 11459-11469.

Quilfen, Y., J. Tournadre, and B. Chapron (2006), Altimeter dual-frequency observations of surface winds, waves, and rain rate in tropical cyclone Isabel, *J. Geophys. Res.*, *111*, C01004, doi:10.1029/2005JC003068.

Reul, N., and B. Chapron (2003), A model of sea-foam thickness distribution for passive microwave remote sensing applications, *J. Geophys. Res., 108*, C10, 3321, doi:10.1029/2003JC001887.

Rose, L.A., W.E. Asher, S.C. Reising, P.W. Gaiser, K.M. St Germain, D.J. Dowgiallo, K.A. Horgan, G. Farquharson, and E.J. Knapp (2002), Radiometric Measurements of the Microwave Emissivity of Foam. *Trans. Geosci. Rem. Sens., 40*, 2619-2625.

Tournadre, J., and Y. Quilfen (2003), Impact of rain cell on scatterometer data: 1. Theory and modelling. *J. Geophys. Res.*, *108*, C7, 3225, doi:10.1029/2002JC001428.

Tournadre, J., and Y. Quilfen (2005), Impact of rain cell on scatterometer data: 2. Correction of Seawinds measured backscatter and wind and rain flagging, *J. Geophys. Res.*, *110*, C07023, doi:10.1029/2004JC002766.

Yueh, S. H., W. J. Wilson, S. J. Dinardo, and S. V. Hsiao (2006), Polarimetric microwave wind radiometer model function and retrieval testing for WindSat, *Trans. Geo. Sc. Remote Sens.*, *44*, 585-595.

WindSat Data Products User's Manual, Version 3.0 (2006), D-29825, Ted Lungu Editor.

	rms (no rain)	mean (no rain)	rms (rain)	mean (rain)	rms (ws>15m/s)	mean (ws>15m/s)
WindSat	1.56	-0.75	3.12	-1.54	2.98	-1.75
WindSat (minus 6GHz)	1.57	-0.75	3.21	-1.53	2.98	-1.71
WindSat (minus 6 and 10 GHz)	2.36	-1.25	3.62	-2.04	4.33	-3.06
WindSat + QuikSCAT	1.73	-0.83	3.00	-1.71	2.90	-1.89
Operational WindSat	2.26	-0.38	8.70	5.54	4.75	-0.49

Table 1: The performance of the inversion for the different observation combinations. The results are first presented for the non-rainy cases (WindSat CLW < 0.2 mm), for the rainy cases, and finally for the wind speeds above 15 m/s. Unit in m/s.

Figure captions

Figure 1: a) Mean QuikSCAT wind speed computed in RP / CLW bins and b) associated number of points, as a function of the rain probability (RP) and cloud liquid water content (CLW).

Figure 2: Distribution of the collocated WindSat / QuikSCAT (solid line) and WindSat / Jason (dashed line) observations as a function of latitude.

Figure 3: Distribution of the wind speeds from the collocated database. Histograms are presented for QuikSCAT, WindSat, and the NCEP model estimates.

Figure 4: Mean Ku-band VV (solid lines) and HH (dashed lines) σ_0 (dB) computed with the RCA model (black), the Kudryavtsev model (blue), and the QuikSCAT data (red), as a function of wind speed (m/s).

Figure 5: Mean Ku-band VV (top panel) and HH (bottom panel) σ_0 (dB) computed with the RCA model (blue) and QuikSCAT data (red), as a function of the wind direction (degrees), for 6 m/s (solid lines), 14 m/s (dashed lines), and 22 m/s (+) mean wind speed.

Figure 6: Mean V-pol (left panels) and H-pol (right panels) Tb's binned as a function of ECMWF wind speed (m/s), at 6.8 GHz (top), 10.7 GHz (middle), and 18.7 GHz (bottom), and for different integrated water vapor ranges: 0mm < WV < 20mm (blue lines), 20mm

< WV < 40mm (black lines), and 40mm < WV < 60mm (red lines). WindSat (dashed lines) and Jason microwave radiometer (dashed lines) integrated water vapor data are used.

Figure 7: Mean V-pol (left panels) and H-pol (right panels) Tb's binned as a function of QuikScat wind speed (m/s), at 6.8 GHz (top), 10.7 GHz (middle), and 18.7 GHz (bottom), and for different integrated water vapor ranges: 0mm < WV < 20mm (solid lines), 20mm < WV < 40mm (dashed lines), and 40mm < WV < 60mm (plus signs). WindSat integrated water vapor data are used.

Figure 8: H-pol Tbs standard deviations binned as a function of QuikSCAT (thin lines) and NCEP (thick lines) wind speed (2 m/s bins), at 6.8 GHz (solid lines), 10.7 GHz (dashed lines), and 18.7 GHz (crosses). The integrated water vapor ranges is 0 mm < WV < 20 mm.

Figure 9: Mean V (left panels) and H (right panels) Tb's binned as a function of QuikSCAT wind speed (m/s), at 6.8 GHz, 10.7 GHz, 18.7 GHz, 23.8 GHz, and 37.0 GHz, respectively from top to bottom, for a dry atmosphere: 0 mm < WV < 20 mm (solid lines), and for a wet atmosphere 20 mm < WV < 60 mm (dashed lines). WindSat data are plotted as blue lines and RTTOV model as red lines.

Figure 10: Mean 3rd (left panels) and 4th (right panels) Stokes parameters binned as a function of the relative wind direction (degrees), at 10.7 GHz (top), 18.7 GHz (middle),

and 37.0 GHz (bottom), and for different wind speed ranges: 4 m/s < WS < 8 m/s (solid lines), 8 m/s < WS < 12 m/s (dashed lines), 12 m/s < WS < 16 m/s (+) , 16 m/s < WS < 20 m/s (o), WS > 20 m/s (red lines). Integrated water vapor is taken in the range WV < 20 mm.

Figure 11: Same as Figure 10 with integrated water vapor taken in the range 20 mm < WV < 50 mm.

Figure 12: Mean 3rd (left panels) and 4th (right panels) Stokes parameters for WindSat (blue lines) and RTTOV-8 model (red lines) binned as a function of the relative wind direction (degrees), at 10.7 GHz (top), 18.7 GHz (middle), and 37.0 GHz (bottom), and for different wind speed ranges: 4 m/s < WS < 8 m/s (solid lines), 12 m/s < WS < 16 m/s (dashed lines), 20 m/s < WS < 24 m/s (dotted lines).

Figure 13: WindSat minus QuikSCAT wind speed difference distribution (top panel), WindSat (middle panel) and QuikSCAT (bottom panel) wind speed distribution for wind speed differences greater than 8 m/s.

Figure 14: Mean WindSat speeds binned by QuikSCAT wind speeds, for 0 mm < WV < 20 mm (solid lines), 20 mm < WV < 40 mm (star), and 40 mm < WV < 80 mm (squares). The thick solid line is the perfect fit line. The bottom curves display the standard deviation of the WindSat minus QuikSCAT differences. WV stands for the WindSat integrated water vapor content. Each bin contains at least 50 collocated measurements.

Figure 15: Mean WindSat speeds binned by Jason winds (left) and ECMWF winds (right), for 0 mm < WV <20 mm (solid lines), 20 mm < WV <40 mm (star signs), and 40 mm < WV < 80 mm (square signs). The thick solid line is the perfect fit line. The bottom curves display the standard deviation of the WindSat minus Jason (left) and ECMWF (right) differences. WV is retrieved from the Jason JMR radiometer. Each bin contains at least 20 points.

Figure 16: Standard deviation (degrees) of the WindSat wind direction minus QuikSCAT (top panel), NCEP (middle panel), ECMWF (bottom panel) wind direction, as a function of wind speed in tropical (thin lines) and mid-latitude areas (thick lines). WV ranges are 0 mm < WV < 20 mm (solid lines) and 20 mm < WV < 80 mm (dashed lines). A minimum of 50 data points is required in each 1 m/s bin.

Figure 17: QuikSCAT (top left) and WindSat (top right) wind fields, speed in m/s, for non rainy areas, in a tropical storm, February 10, 2003, 12h00 UTC. WindSat integrated water vapor content (bottom left in mm) and rain rate (bottom right in mm/hr).

Figure 18: Wind speed errors for different combinations of observations, stratified by the QuikSCAT wind speed taken as a reference. For each combination, the rms and mean errors calculated over the original data set (including rainy pixels) are indicated.

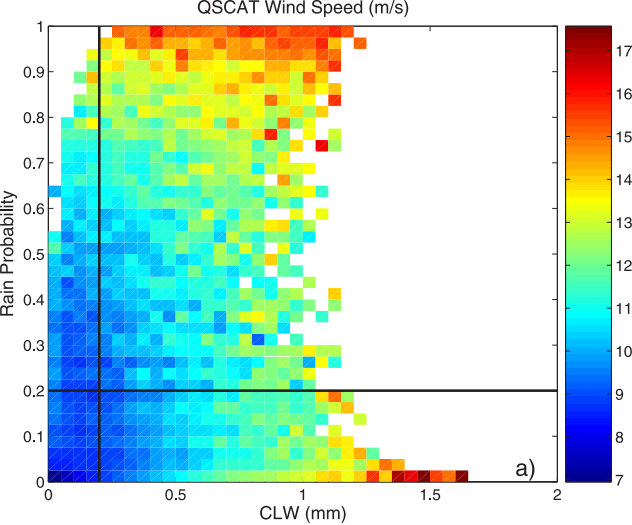
QSCAT Wind Speed (m/s)
Rain Probability
CLW (mm)
a)
0
0.1
0.2
0.3
0.4
0.5
0.6
0.7
0.8
0.9
1
0.5
1.5
2
7
8
9
10
11
12
13
14
15
16
17

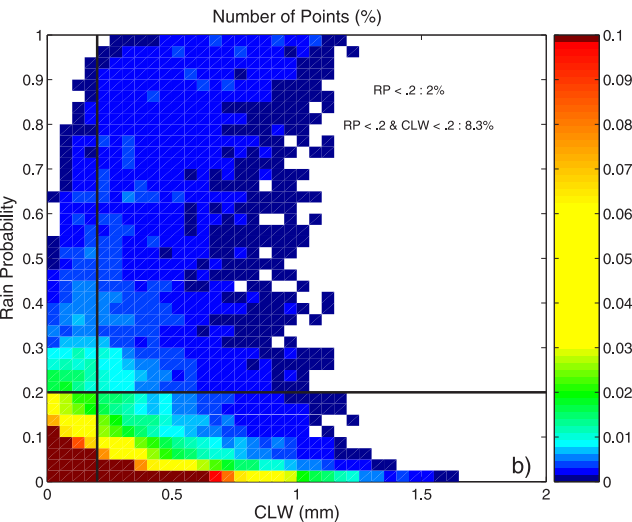
Number of Points (%)
RP < .2 : 2%
RP < .2 & CLW < .2 : 8.3%
Rain Probability
CLW (mm)
b)
0
0.1
0.2
0.3
0.4
0.5
0.6
0.7
0.8
0.9
1
0.5
1
1.5
2
0.01
0.02
0.03
0.04
0.05
0.06
0.07
0.08
0.09
0.1

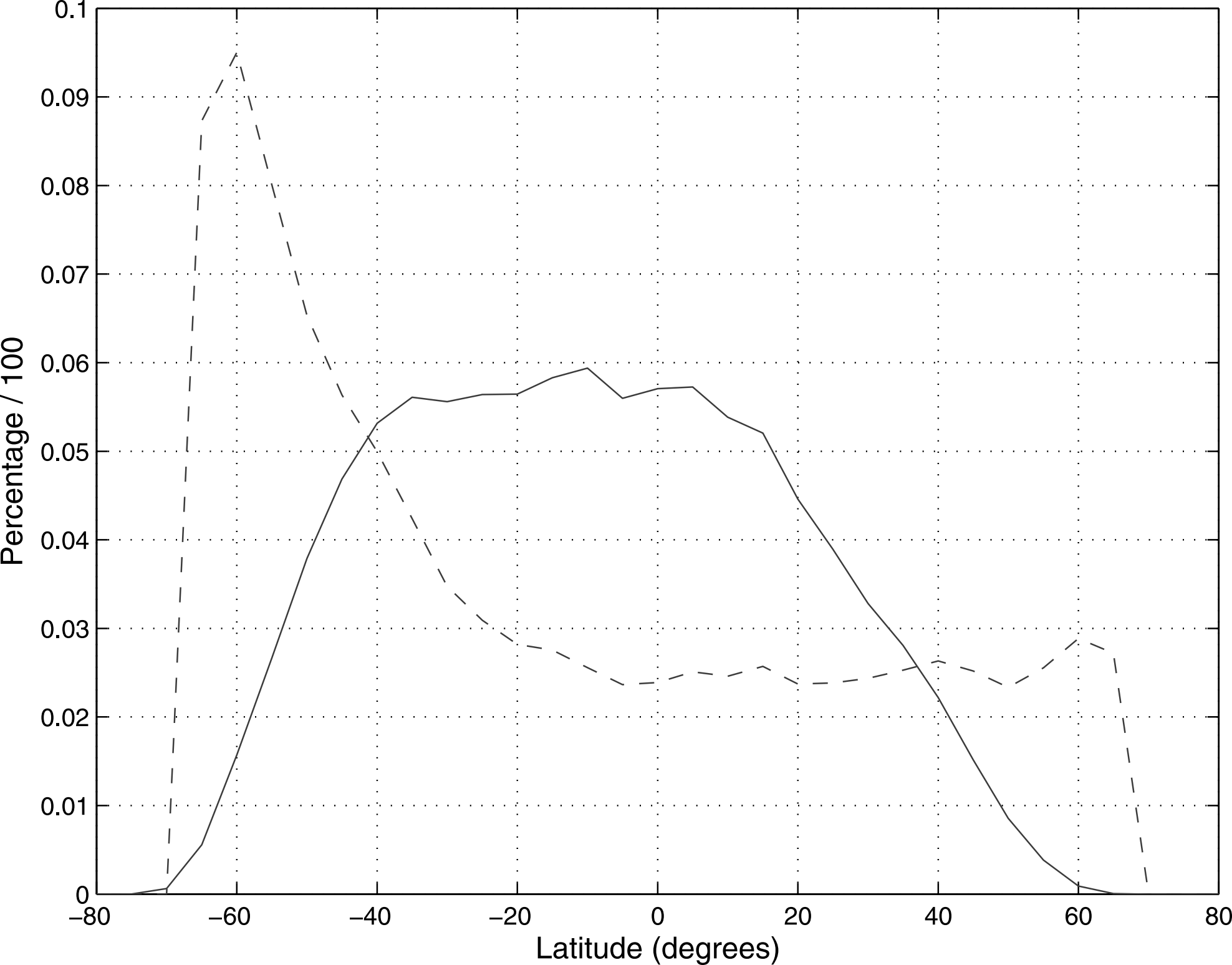
0.1
0.09
0.08
0.07
0.06
0.05
0.04
0.03
0.02
0.01
0
Percentage / 100
−80
−60
−40
−20
0
20
40
60
80
Latitude (degrees)

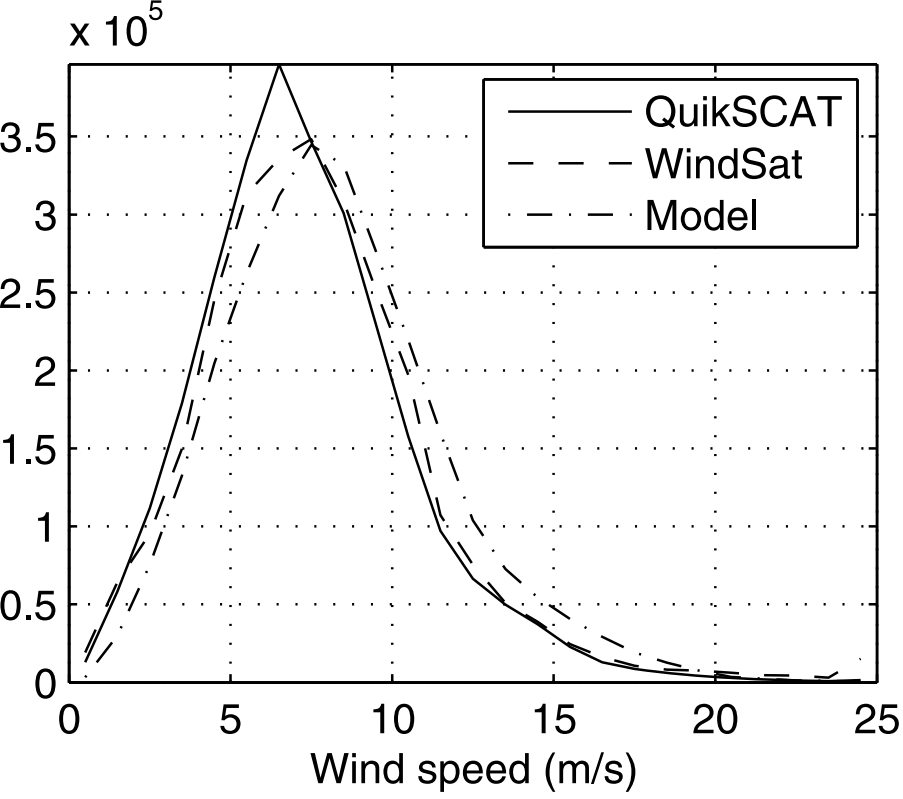
x 10^5
QuikSCAT
WindSat
Model
3.5
3
2.5
2
1.5
1
0.5
0
0
5
10
15
20
25
Wind speed (m/s)

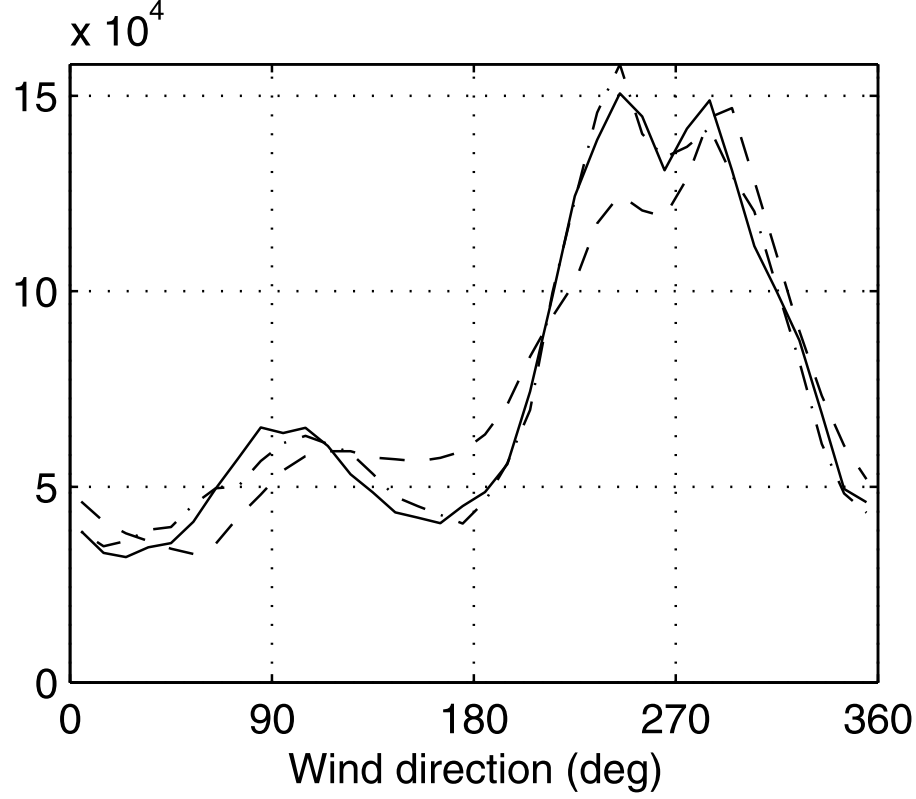
x 10^4
15
10
5
0
0
90
180
270
360
Wind direction (deg)

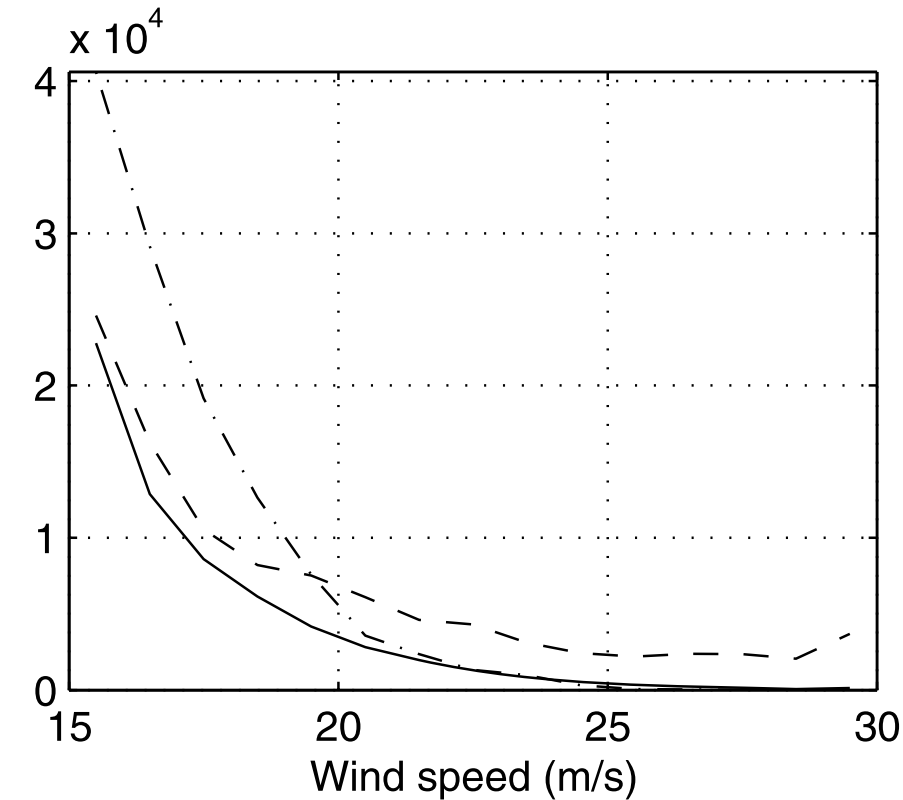
x 10^4
4
3
2
1
0
15
20
25
30
Wind speed (m/s)

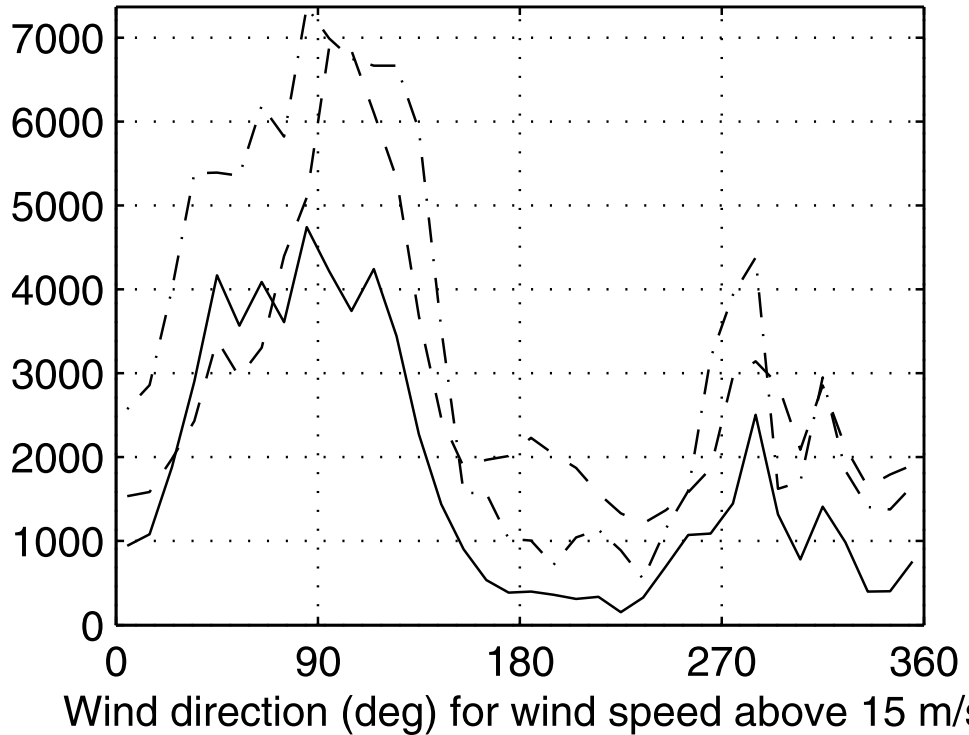
7000
6000
5000
4000
3000
2000
1000
0
0
90
180
270
360
Wind direction (deg) for wind speed above 15 m/s

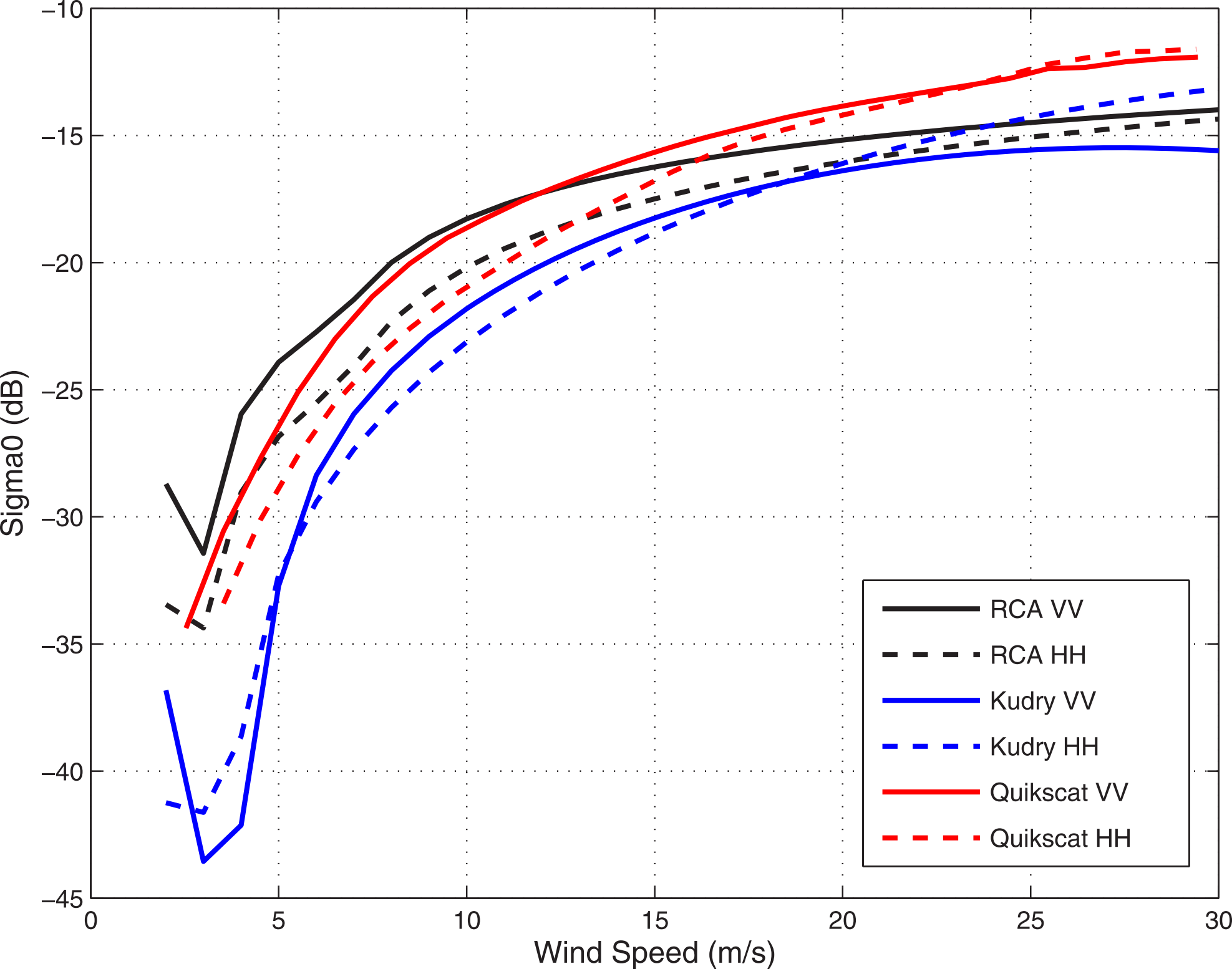
−10
−15
−20
−25
−30
−35
−40
−45
Sigma0 (dB)
0
5
10
15
20
25
30
Wind Speed (m/s)
RCA VV
RCA HH
Kudry VV
Kudry HH
Quikscat VV
Quikscat HH

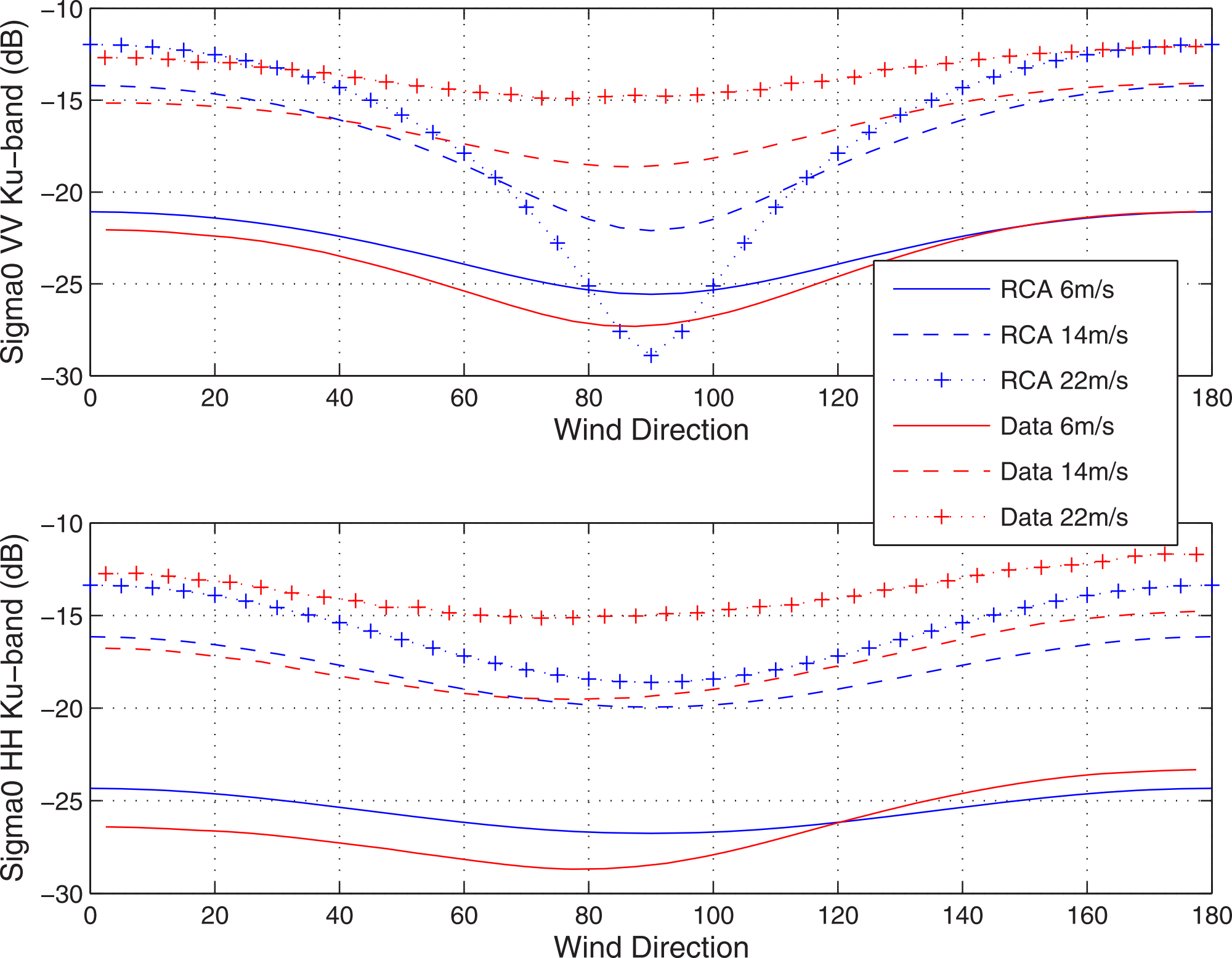
Sigma0 VV Ku−band (dB)
−10
−15
−20
−25
−30
0
20
40
60
80
100
120
180
Wind Direction
RCA 6m/s
RCA 14m/s
RCA 22m/s
Data 6m/s
Data 14m/s
Data 22m/s
Sigma0 HH Ku−band (dB)
−10
−15
−20
−25
−30
0
20
40
60
80
100
120
140
160
180
Wind Direction

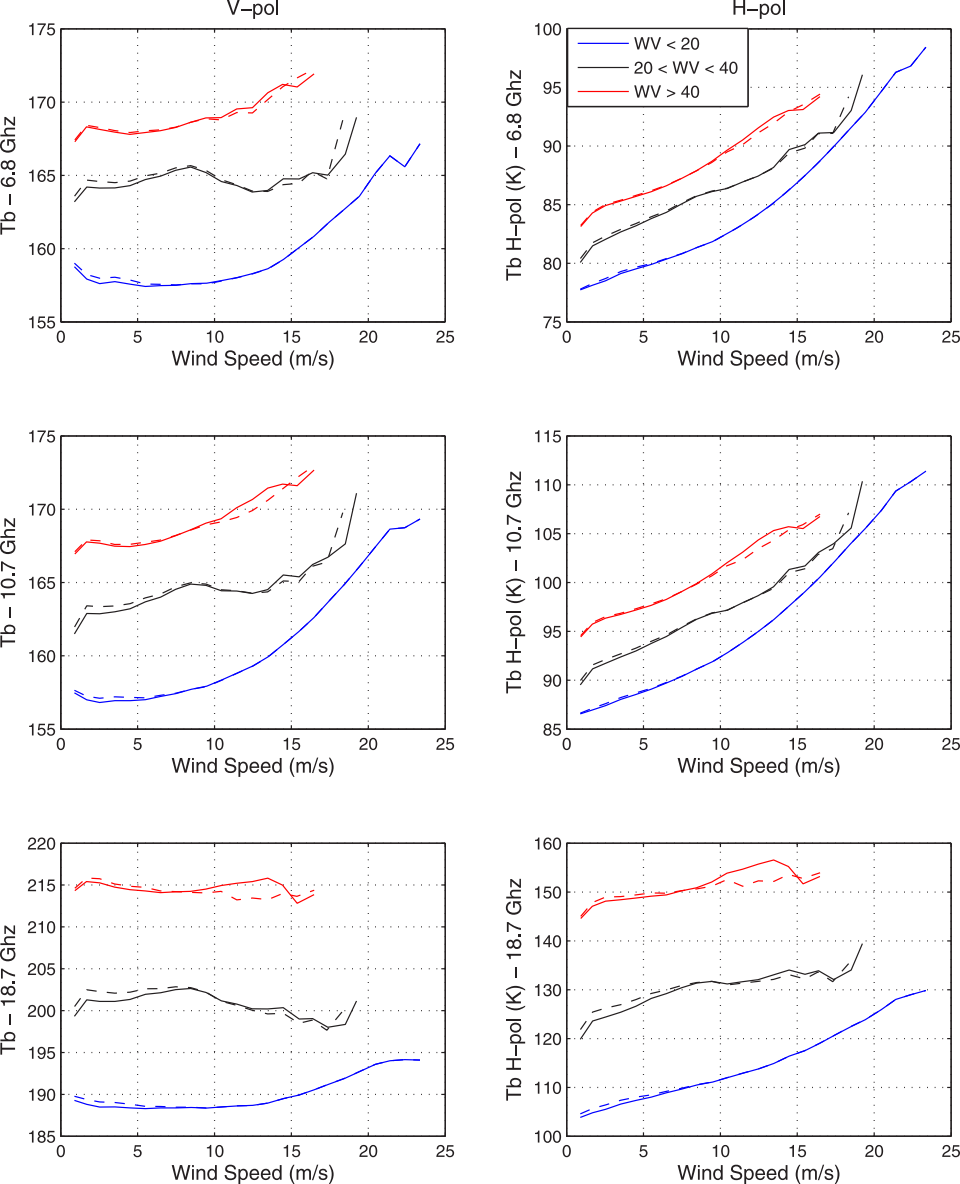
V–pol
H–pol
WV < 20
20 < WV < 40
WV > 40
Tb – 6.8 Ghz
Tb H–pol (K) – 6.8 Ghz
Tb – 10.7 Ghz
Tb H–pol (K) – 10.7 Ghz
Tb – 18.7 Ghz
Tb H–pol (K) – 18.7 Ghz
Wind Speed (m/s)

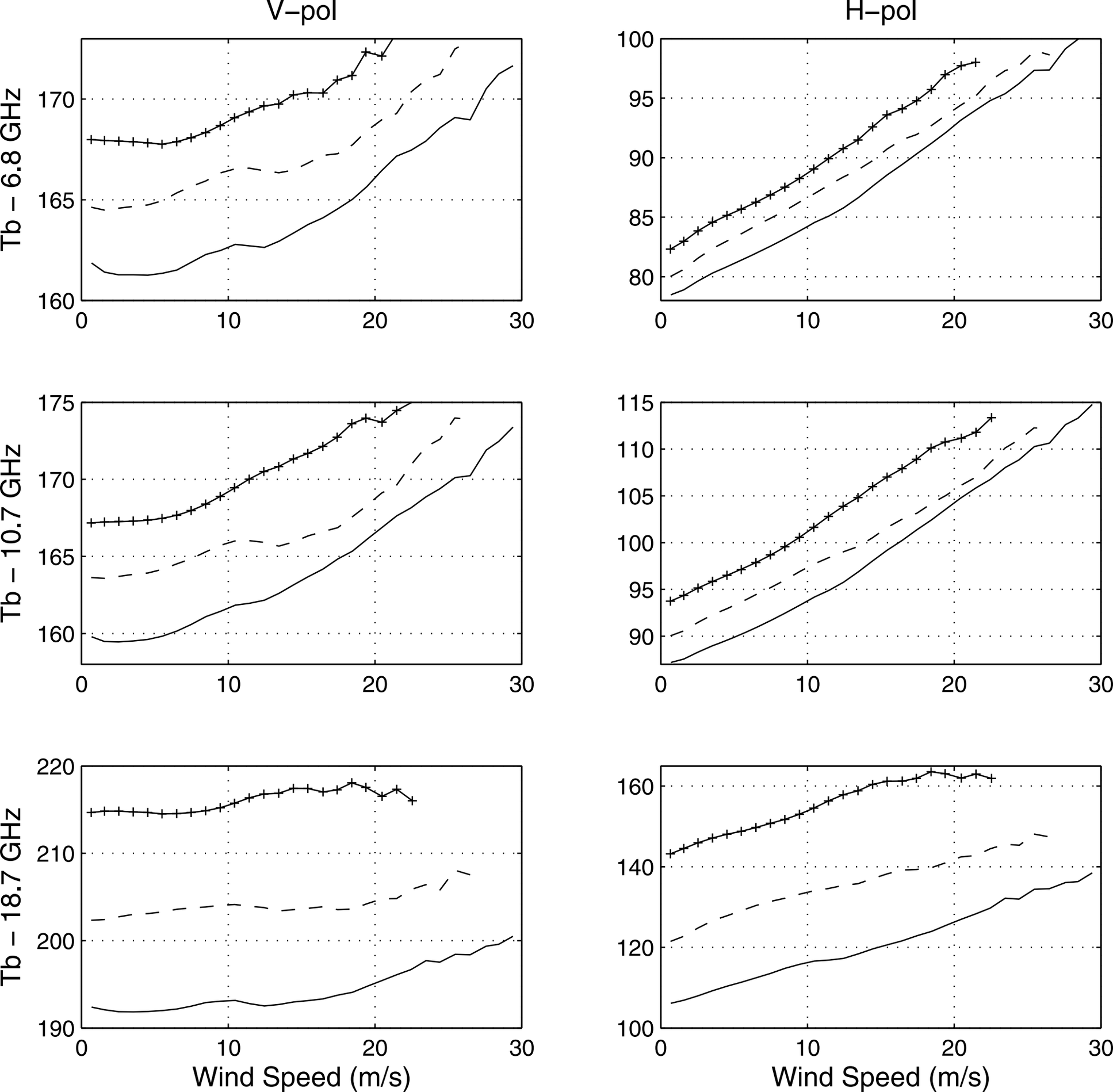
V–pol
H–pol
Tb – 6.8 GHz
Tb – 10.7 GHz
Tb – 18.7 GHz
Wind Speed (m/s)
Wind Speed (m/s)

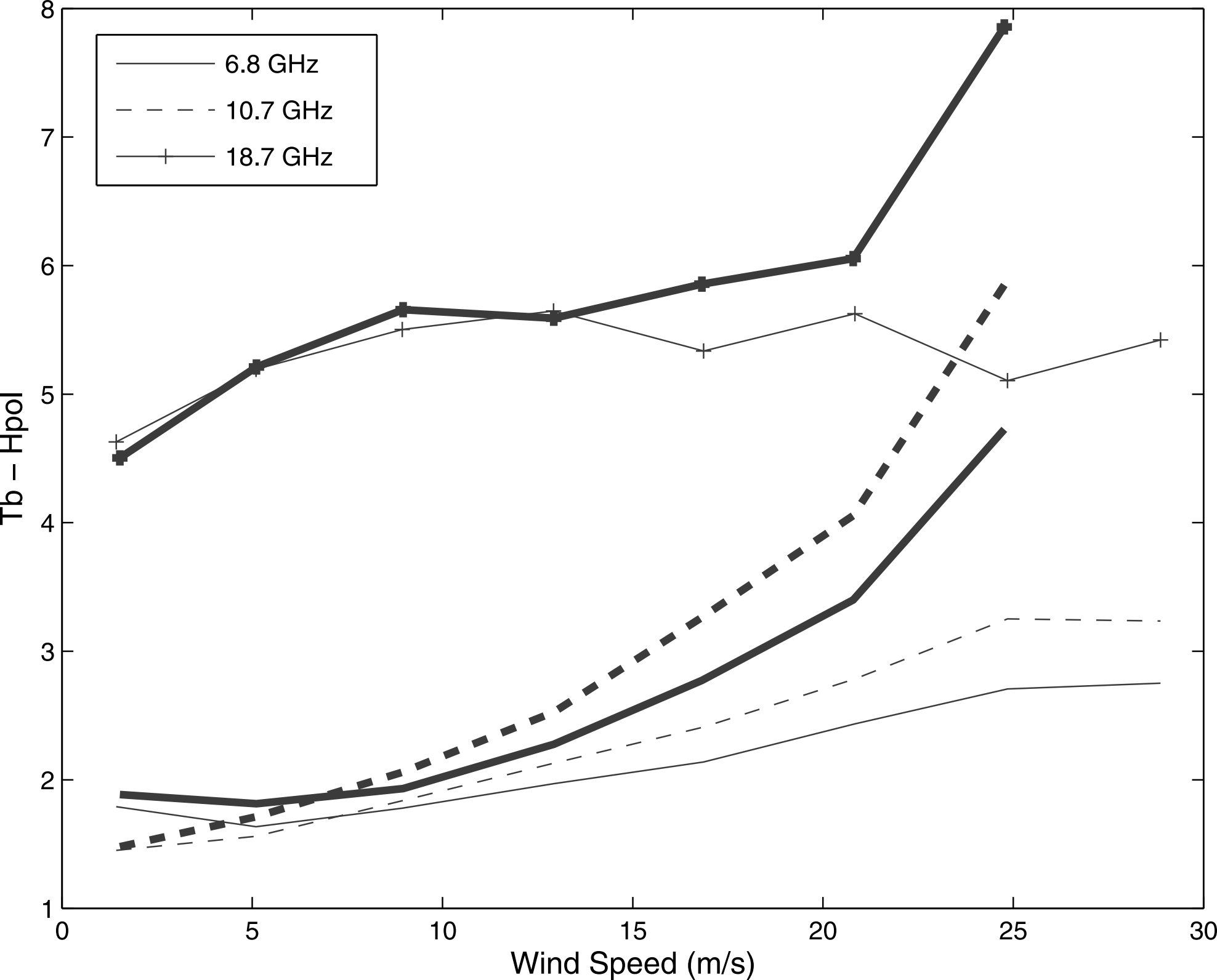
6.8 GHz
10.7 GHz
18.7 GHz
Tb – Hpol
Wind Speed (m/s)
1
2
3
4
5
6
7
8
0
5
10
15
20
25
30

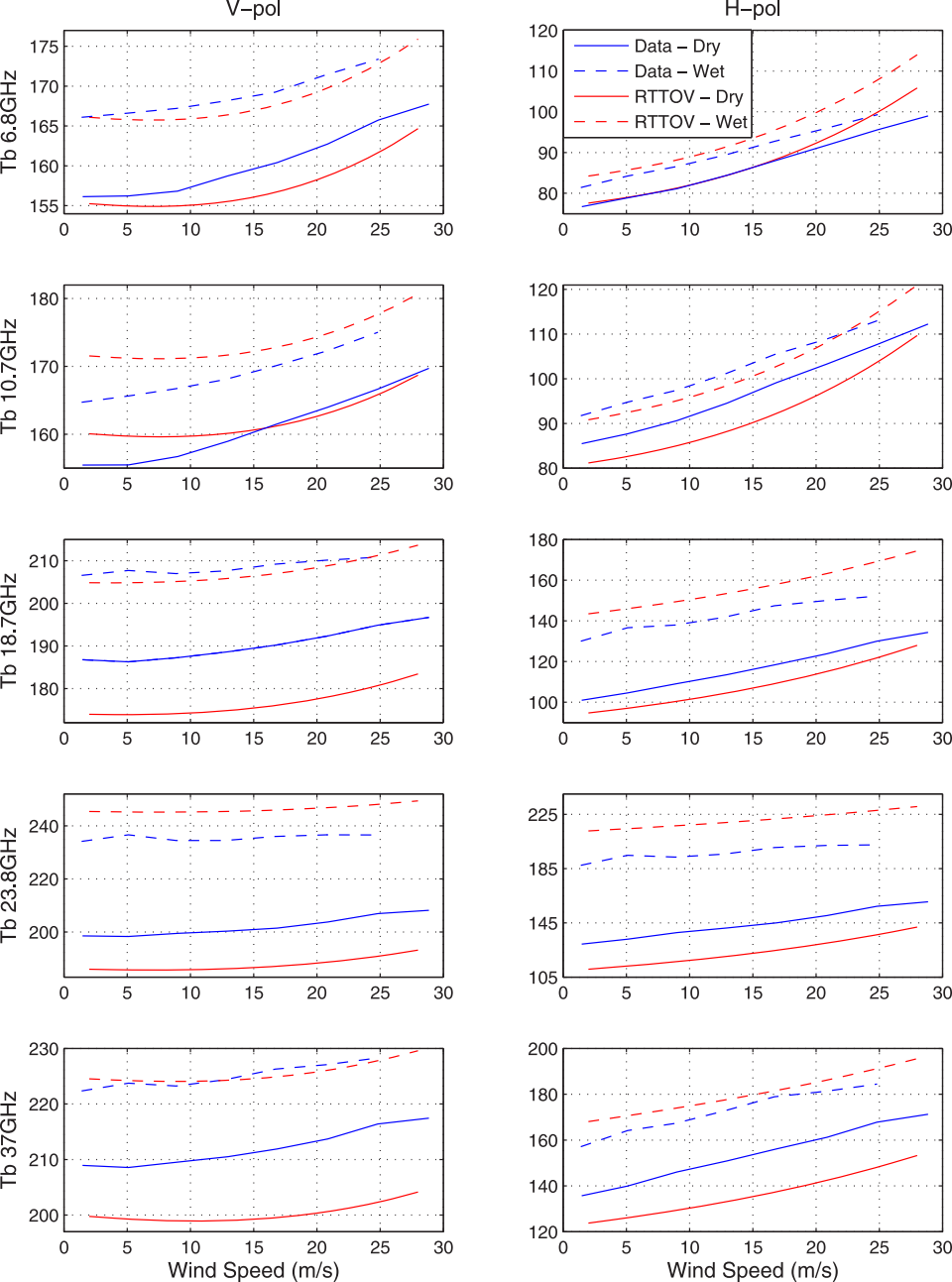
V–pol
H–pol
Data – Dry
Data – Wet
RTTOV – Dry
RTTOV – Wet
Tb 6.8GHz
Tb 10.7GHz
Tb 18.7GHz
Tb 23.8GHz
Tb 37GHz
Wind Speed (m/s)
Wind Speed (m/s)

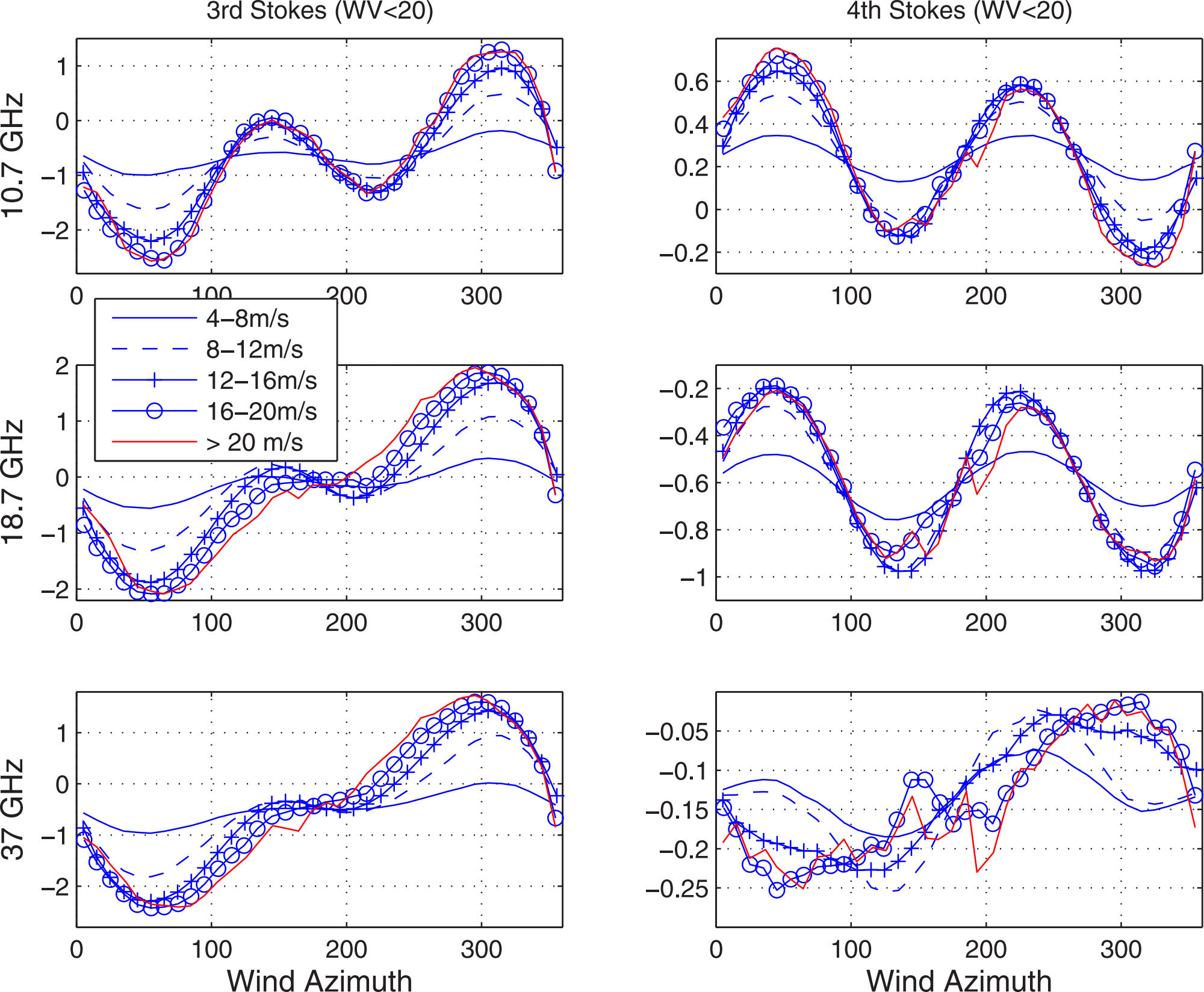
3rd Stokes (WV<20)
4th Stokes (WV<20)
10.7 GHz
18.7 GHz
37 GHz
4–8m/s
8–12m/s
12–16m/s
16–20m/s
> 20 m/s
Wind Azimuth
Wind Azimuth

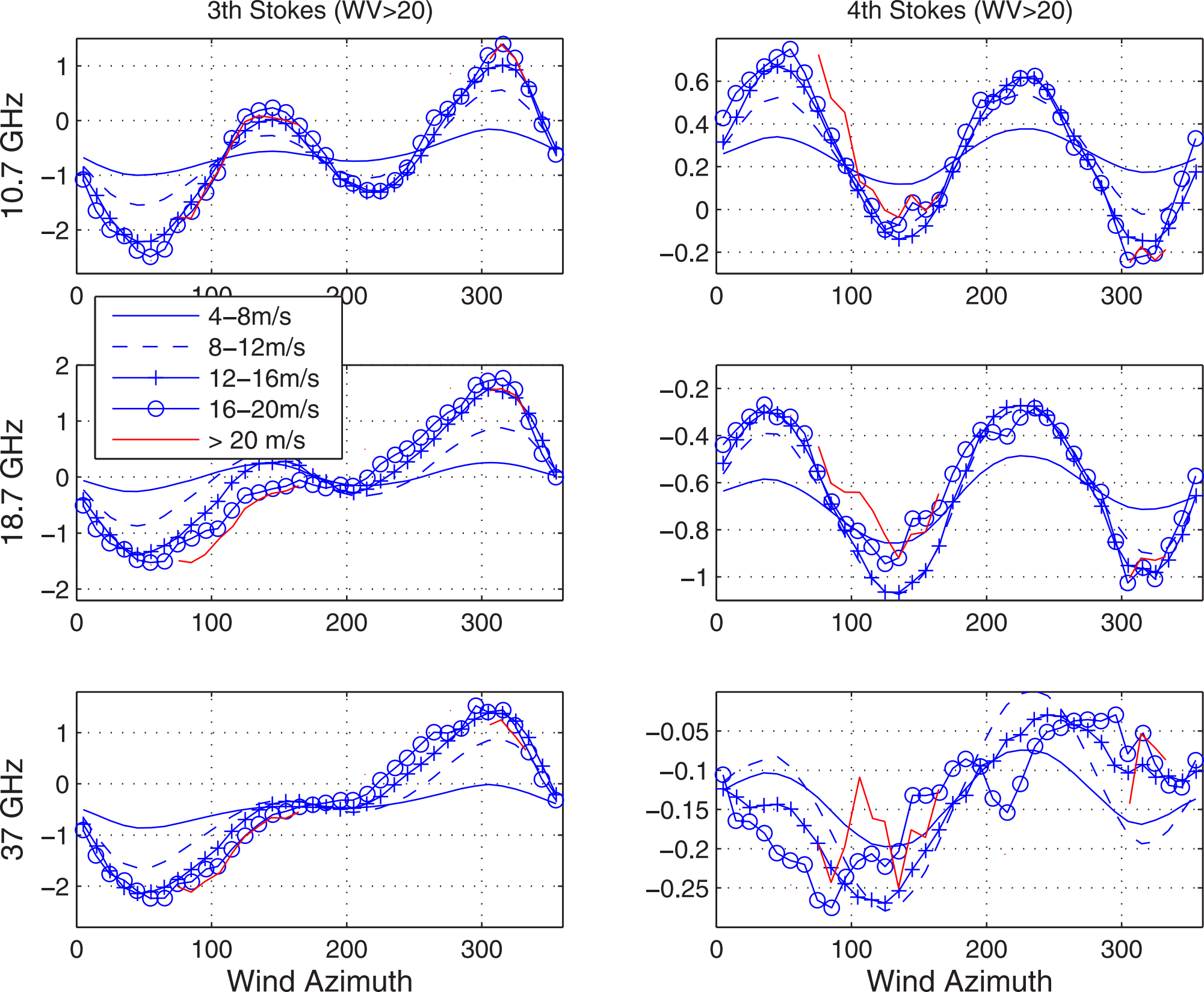
3th Stokes (WV>20)
4th Stokes (WV>20)
10.7 GHz
18.7 GHz
37 GHz
4–8m/s
8–12m/s
12–16m/s
16–20m/s
> 20 m/s
Wind Azimuth
Wind Azimuth

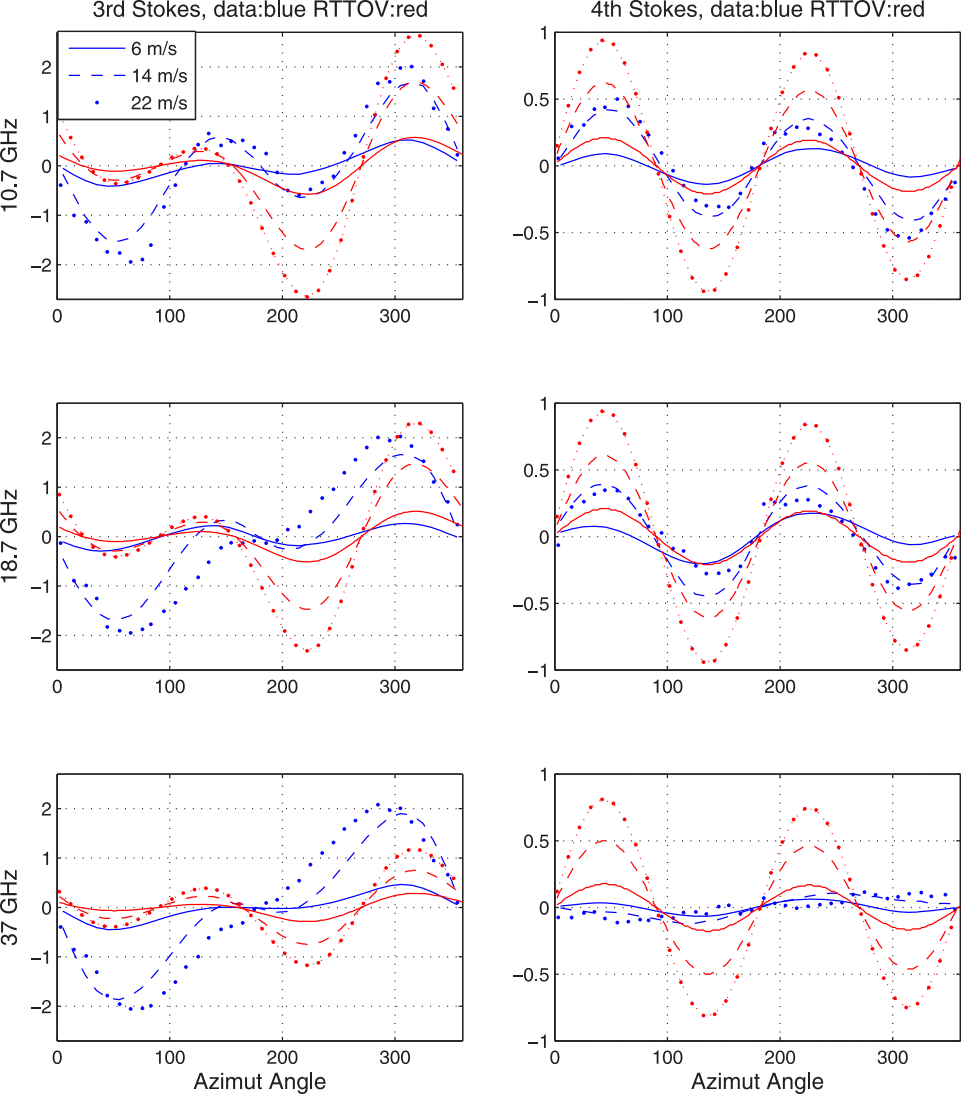
3rd Stokes, data:blue RTTOV:red
4th Stokes, data:blue RTTOV:red
6 m/s
14 m/s
22 m/s
10.7 GHz
18.7 GHz
37 GHz
Azimut Angle
Azimut Angle

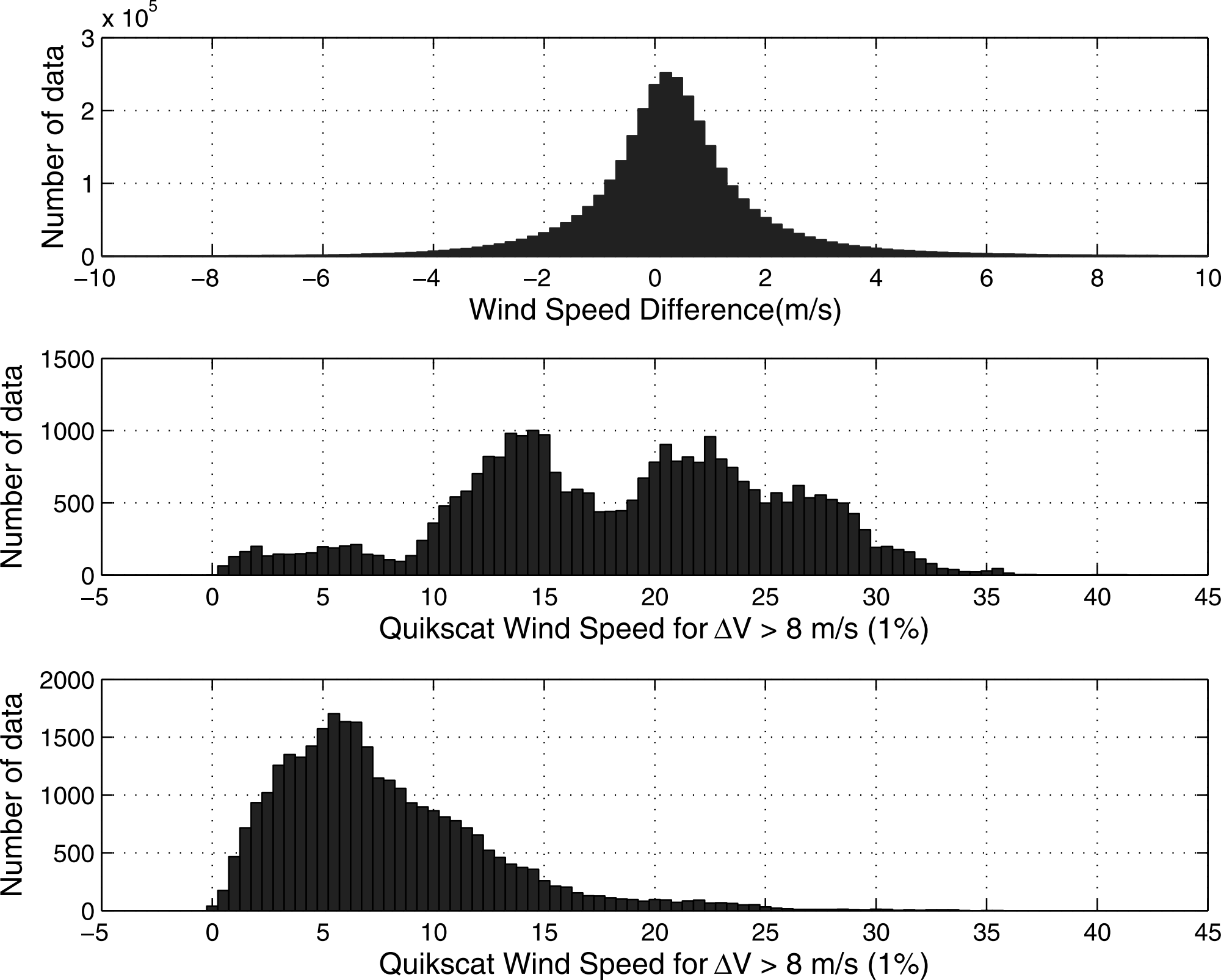
x 10^5
Number of data
Wind Speed Difference(m/s)
Number of data
Quikscat Wind Speed for ΔV > 8 m/s (1%)
Number of data
Quikscat Wind Speed for ΔV > 8 m/s (1%)

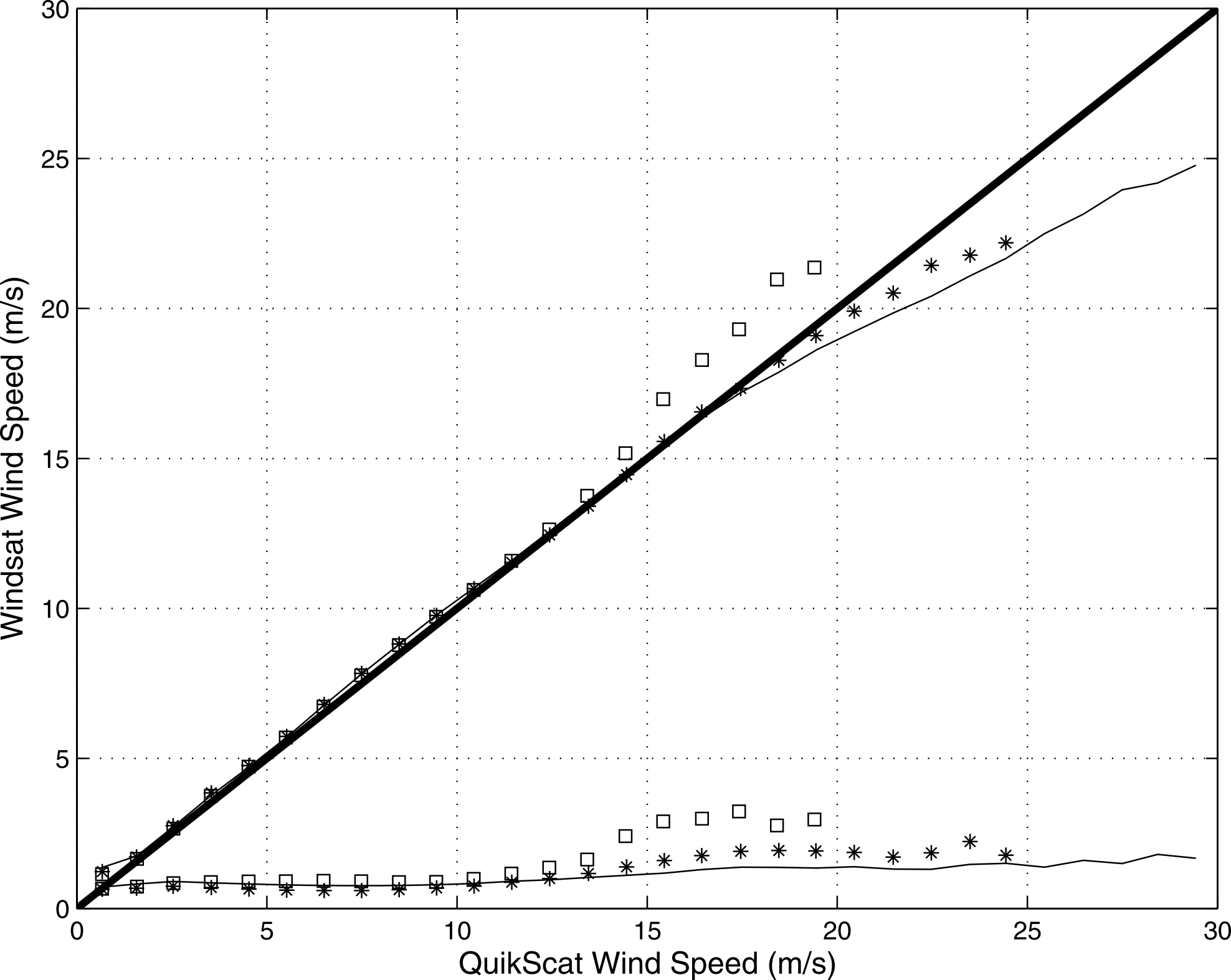
Windsat Wind Speed (m/s)
QuikScat Wind Speed (m/s)
0
5
10
15
20
25
30

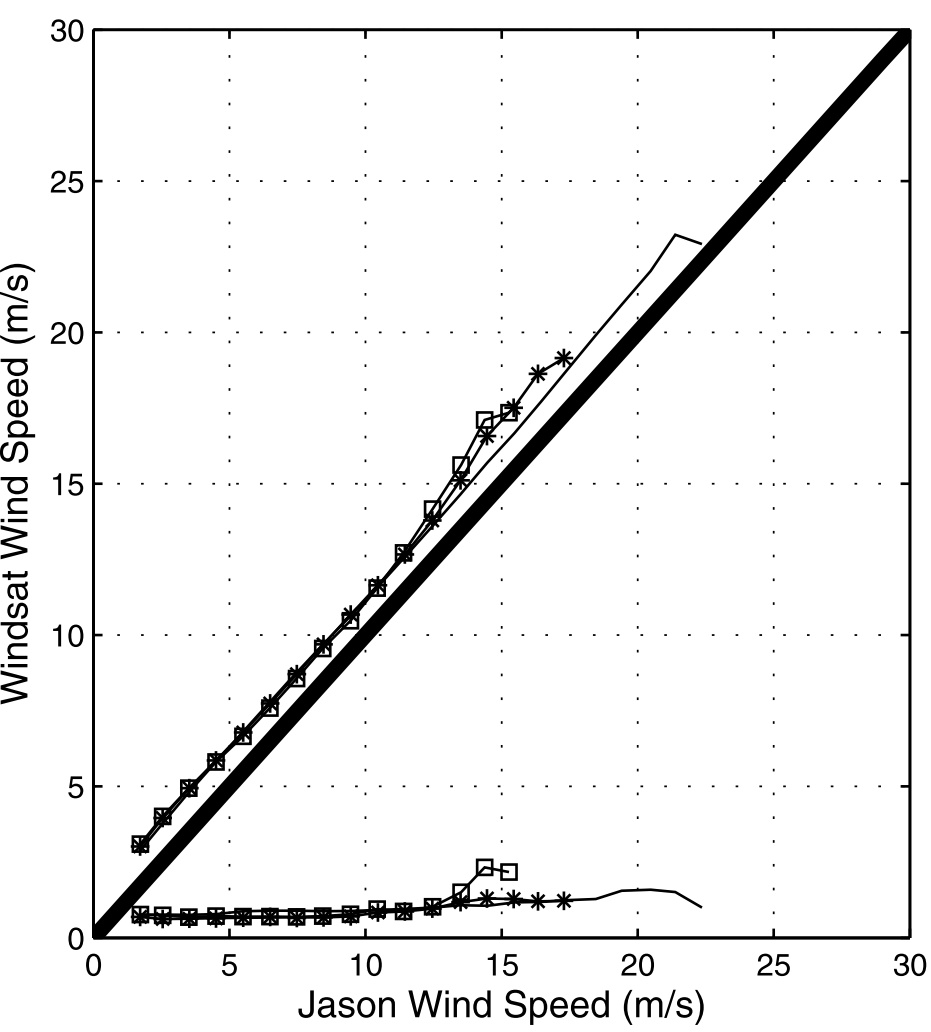
Windsat Wind Speed (m/s)
Jason Wind Speed (m/s)
0
5
10
15
20
25
30

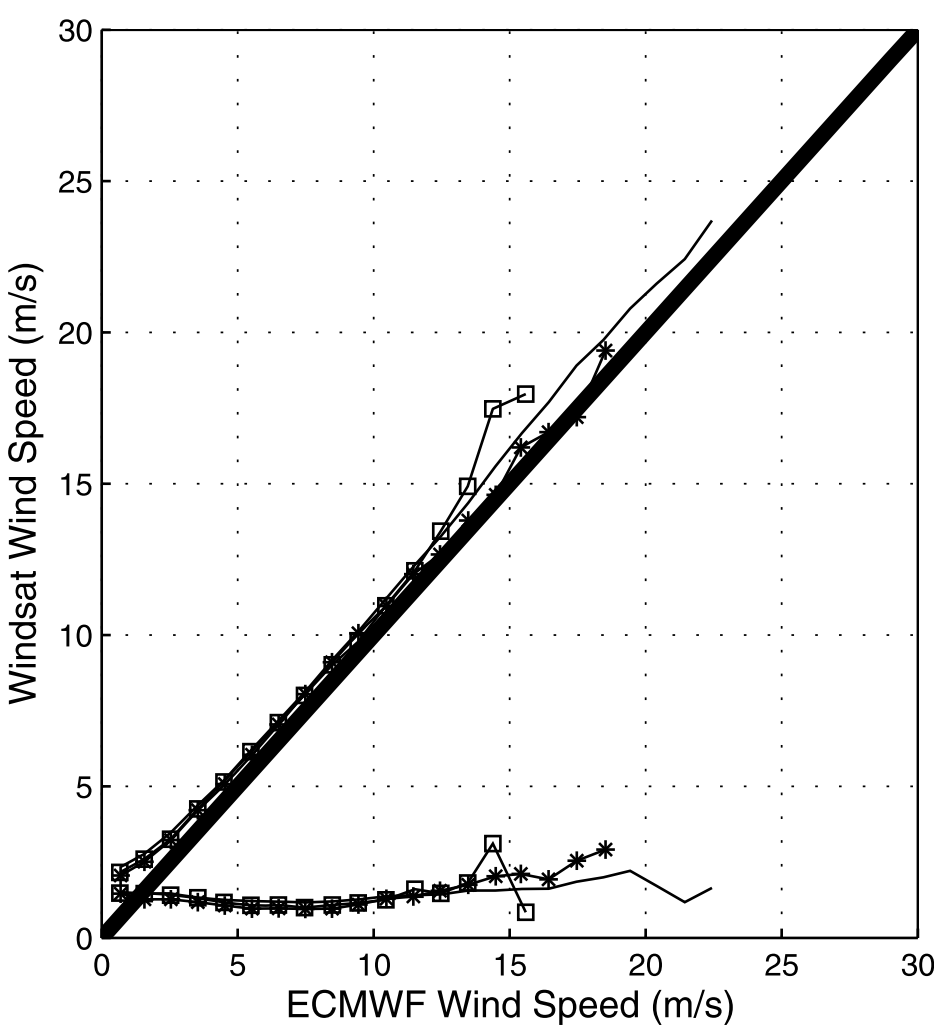
Windsat Wind Speed (m/s)
ECMWF Wind Speed (m/s)
0
5
10
15
20
25
30

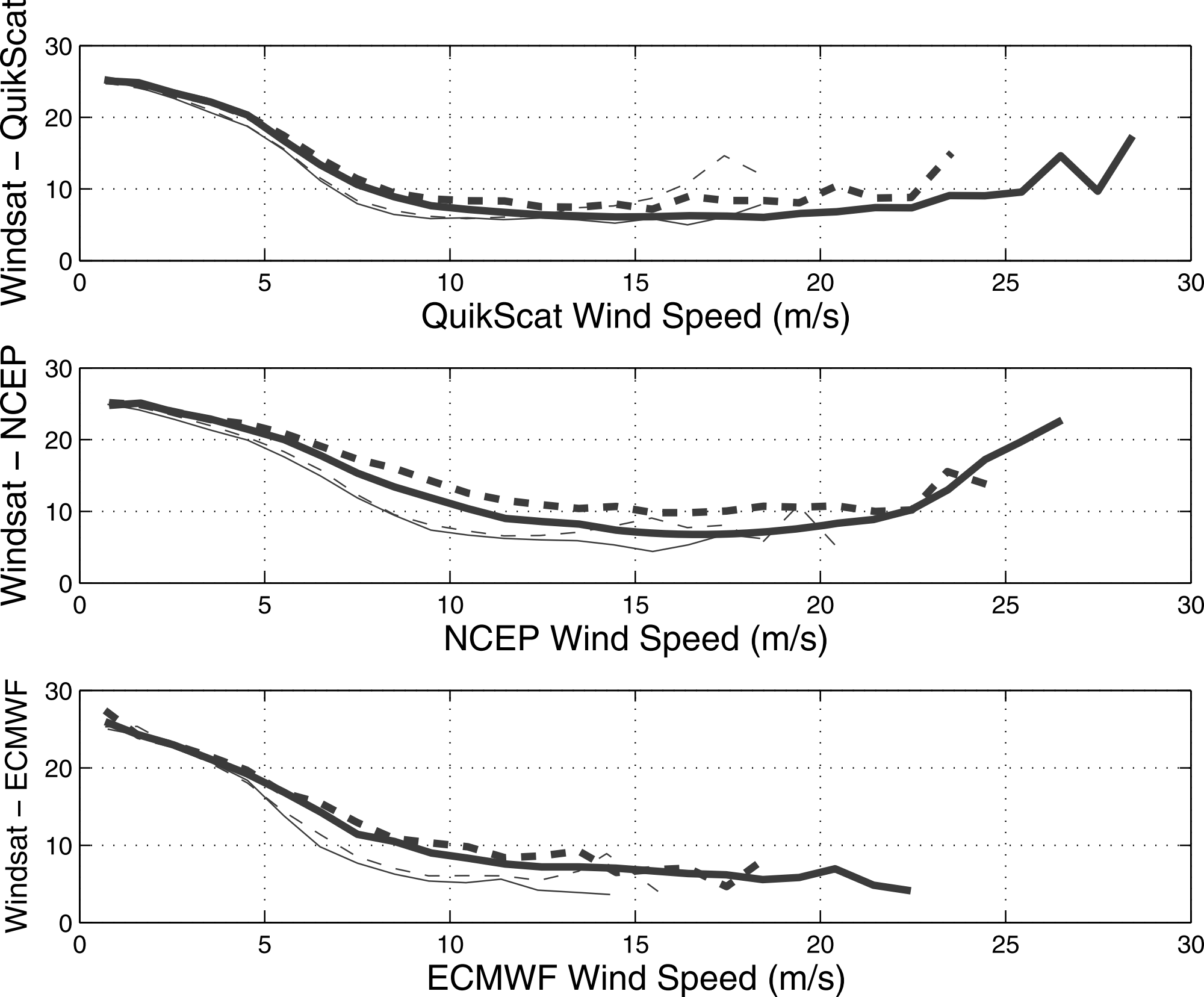
Windsat – QuikScat
QuikScat Wind Speed (m/s)
Windsat – NCEP
NCEP Wind Speed (m/s)
Windsat – ECMWF
ECMWF Wind Speed (m/s)
0
5
10
15
20
25
30

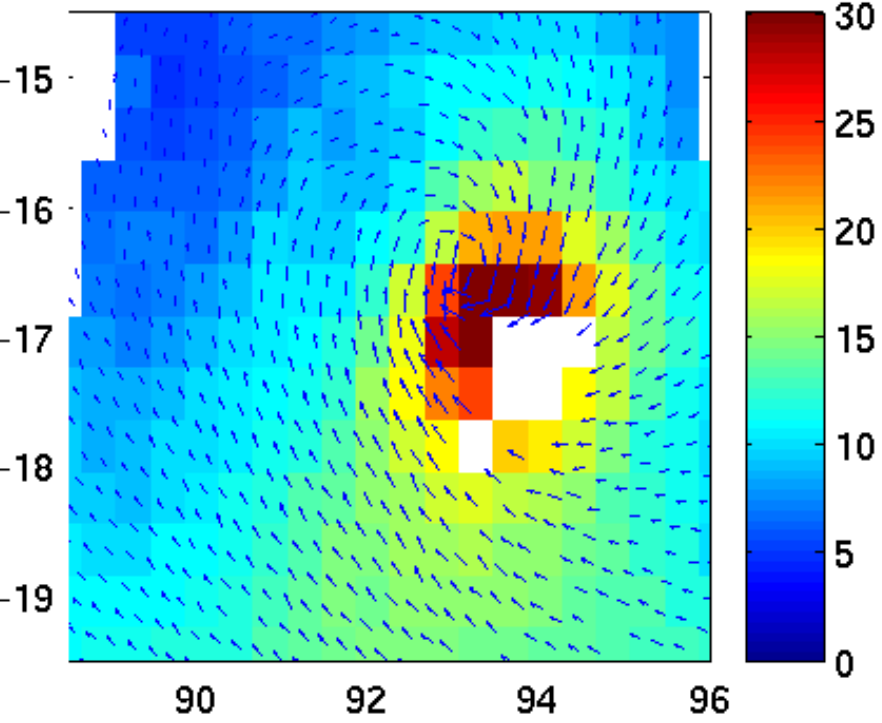
-15
-16
-17
-18
-19
90
92
94
96
30
25
20
15
10
5
0

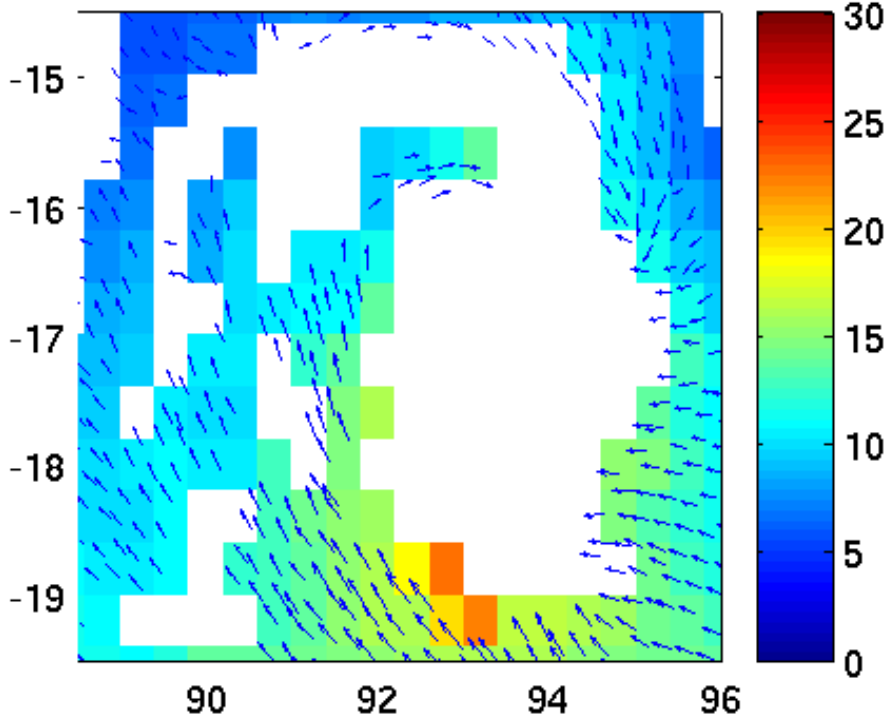
-15
-16
-17
-18
-19
90
92
94
96
30
25
20
15
10
5
0

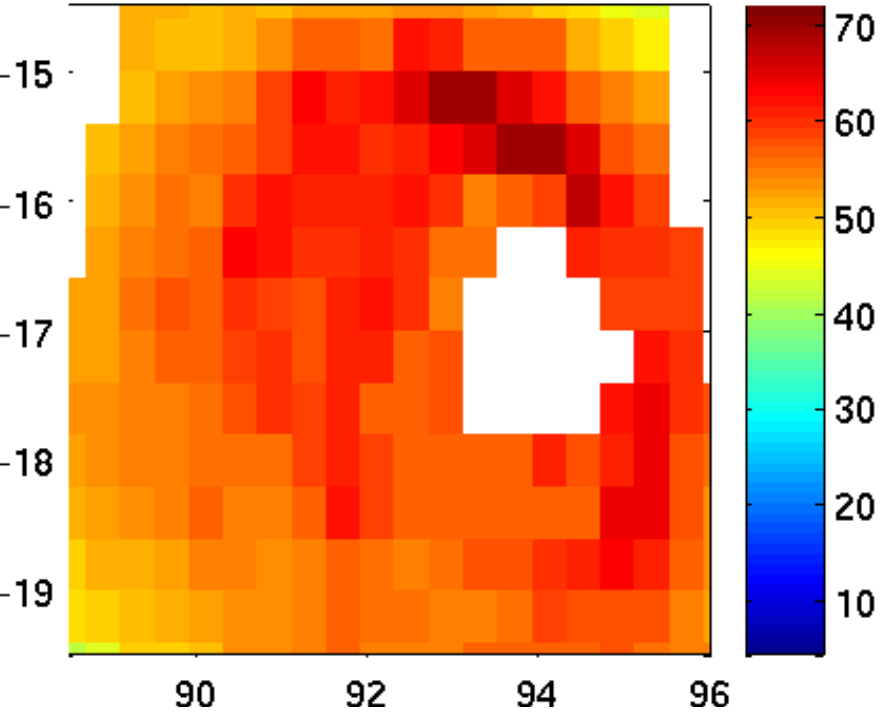
-15
-16
-17
-18
-19
90
92
94
96
70
60
50
40
30
20
10

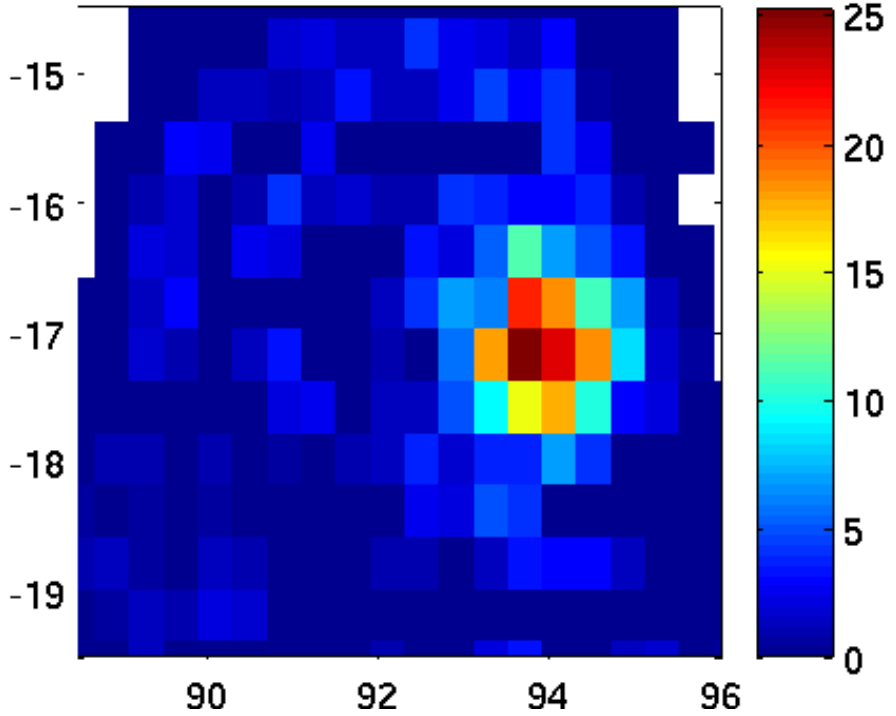
-15
-16
-17
-18
-19
90
92
94
96
25
20
15
10
5
0

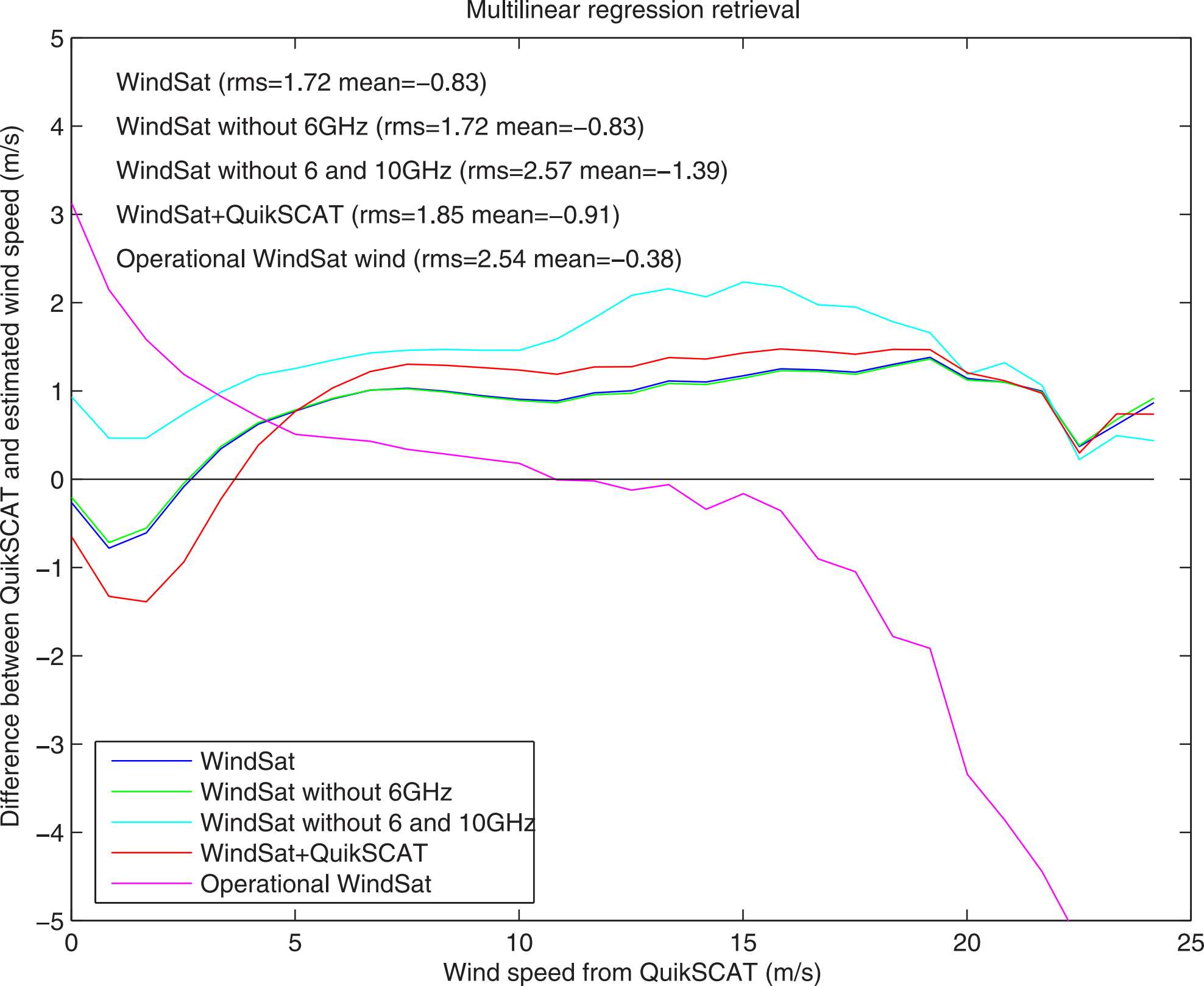
Multilinear regression retrieval
WindSat (rms=1.72 mean=–0.83)
WindSat without 6GHz (rms=1.72 mean=–0.83)
WindSat without 6 and 10GHz (rms=2.57 mean=–1.39)
WindSat+QuikSCAT (rms=1.85 mean=–0.91)
Operational WindSat wind (rms=2.54 mean=–0.38)
WindSat
WindSat without 6GHz
WindSat without 6 and 10GHz
WindSat+QuikSCAT
Operational WindSat
Difference between QuikSCAT and estimated wind speed (m/s)
Wind speed from QuikSCAT (m/s)
5
4
3
2
1
0
−1
−2
−3
−4
−5
0
5
10
15
20
25